# Chapter 4

# Results of Model Calculations

## 4.1 Predictions for Typical Tokamak Plasmas

In order to investigate the diagnostic potential of fast He beams, extensive modelling calculations of the development of He ground state- and metastable states populations and the resulting intensity profiles of HeI lines of interest for a fast He beam penetrating a plasma have been performed. The profiles of all HeI lines in the optical region have been calculated, i.e. 6 singlet- and 5 triplet lines (see figure 3.2). We used electron density- and temperature profiles taken from ASDEX Upgrade- and JET measurements by the respective standard diagnostics. Calculations have been performed for incident pure $1^1S$ and pure $2^3S$ beams, respectively. The results for a beam with an initial metastable fraction between those two extremes can be determined by mixing the two results with the corresponding weight factors. The beam energy was taken in accordance with the energy available for our first experiments at these devices. A neutral beam current of 1 A uniformly distributed over a diameter of 0.1 m ($\hat{=}$ 127 A/m$^2$) was assumed. With these calculations, predictions for first experiments with fast He beams at Tokamak plasmas (ASDEX Upgrade and JET, see chapter 5) in view of beam attenuation, necessary beam intensity, and the most intense visible lines have been made. Also, we focussed our attention on the redistribution of the initial metastable fraction. A detailed presentation of the calculation results has been given in [89]. In the next subchapters the essential results are discussed.

### 4.1.1 ASDEX Upgrade Plasma

For ASDEX Upgrade ('AUG'), we have chosen the L-mode discharge #11277 with a line averaged density of $8{\cdot}10^{19}$ $m^{-2}$ and a peak electron temperature of 1.8 keV as input for our modelling. The calculations have been performed for an initial beam composition of pure ground state and pure metastable triplet state, respectively.

#### 4.1.1.1 AUG Plasma Edge

The $T_e$- and $n_e$ profiles used for the AUG plasma-edge calculations are shown in figure 4.1. The modelling parameters are as follows:

| | |
|---|---|
| beam energy | 30 keV |
| initial equivalent He beam current | 1 A |
| beam diameter | 0.1 m |
| $T_e$ at separatrix | 75 eV |
| $T_e$ decay length | 10 mm |
| minimum $T_e$ value | 4 eV [19] (reached for a penetration depth $\leq$ 0.07 m, see figure 4.1) |
| $n_e$ at separatrix | $4{\cdot}10^{19}$ $m^{-3}$ |
| $n_e$ decay length | 30 mm |
| number of calculation steps | 200 |
| penetration depth | 0.1 m |

The results for population density- and line intensity profiles for an initially pure ground-state beam are given in figures 4.2 to 4.4. At the separatrix 1% of the initial beam intensity is attenuated, see figure 4.2. The rise of $T_e$ at 70 mm penetration depth has a definite influence on the $2^3S$ population. Its behaviour is quite similar to the corresponding triplet-line profiles (see figure 4.3). Figure 4.4 shows the singlet line-intensity profiles for the initially pure ground-state beam. The 728 nm-line intensity profile reflects the progression of the $2^1S$ population, whereas all other singlet lines show a stronger dependence on the electron-temperature profile. All line profiles for both spin systems show good reproduction of the exponential rise of the electron density in the region with constant electron temperature (penetration depth: 0 to 70 mm).

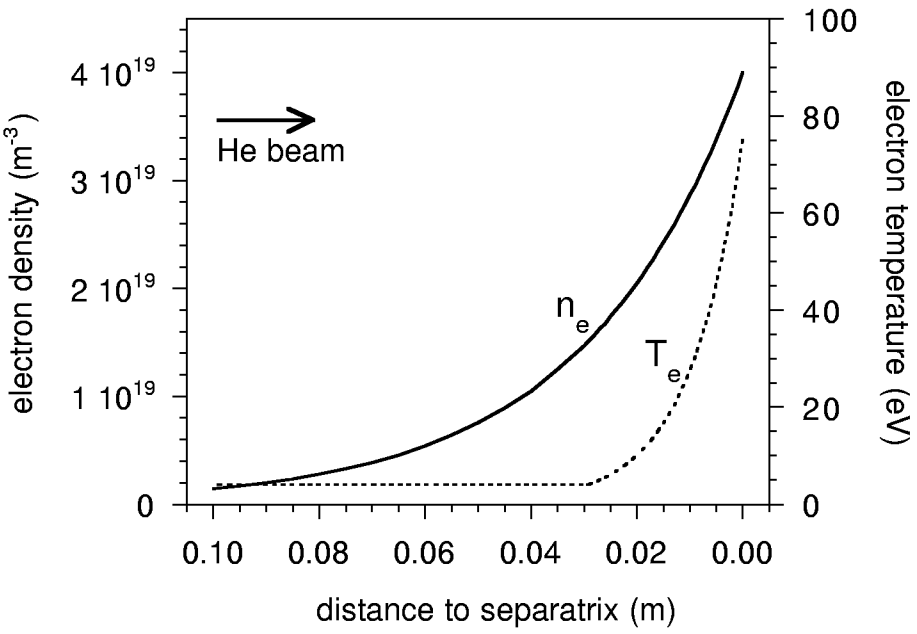


**Figure 4.1:** $n_e$- and $T_e$ profiles used for the modelling calculations for a typical AUG edge plasma (discharge #11277).

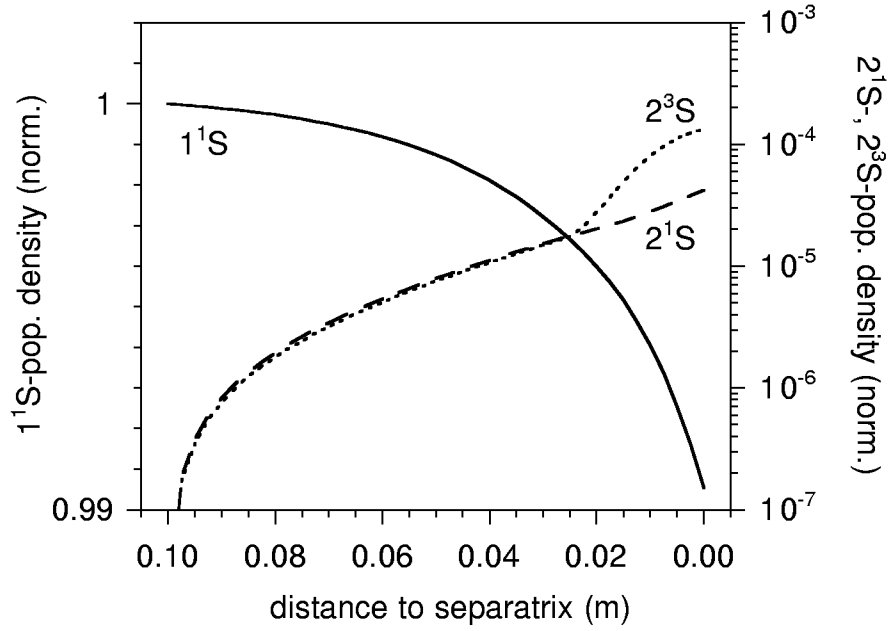


**Figure 4.2:** Progression of the $1^1$S-, $2^1$S-, and $2^3$S populations for an initially pure $1^1$S beam (normalized to the initial beam intensity). The modelling is based on AUG discharge #11277 and a 1 A / 30 keV He beam with 0.1 m diameter.

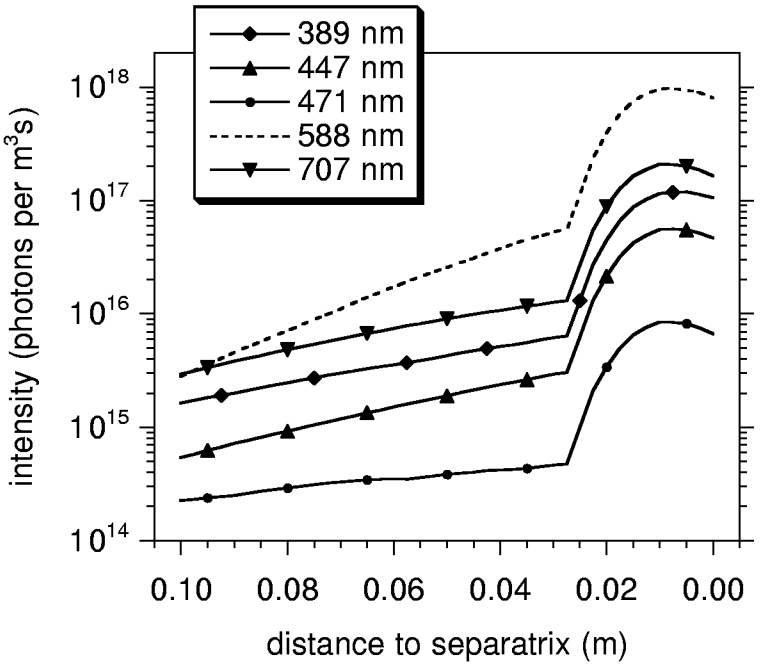


**Figure 4.3:** Progression of optical HeI-triplet lines for an initially pure $1^1S$ beam. The modelling is based on AUG discharge #11277 and a 1 A / 30 keV He beam with 0.1 m diameter.

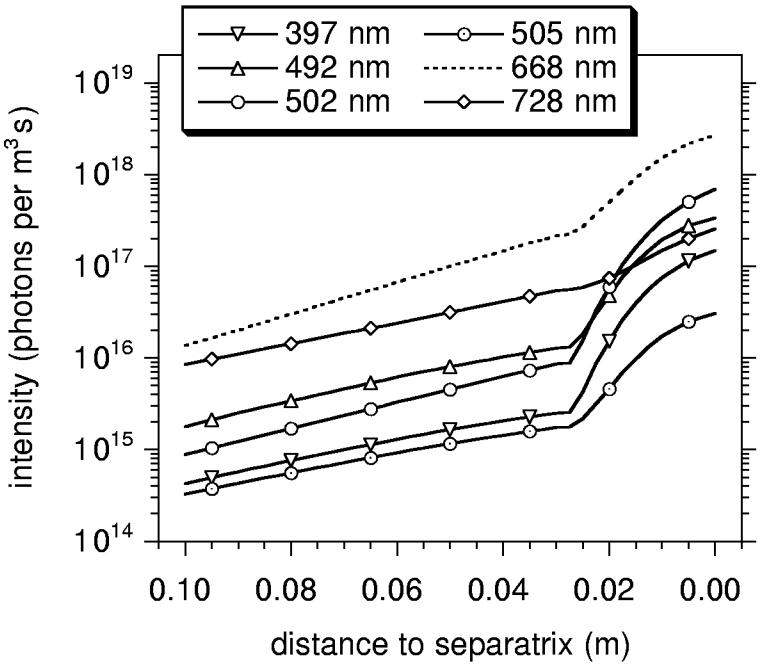


**Figure 4.4:** Progression of optical HeI-singlet lines for an initially pure $1^1S$ beam. The modelling is based on AUG discharge #11277 and a 1 A / 30 keV He beam with 0.1 m diameter.

The results for population density- and line-intensity profiles for an initially pure $2^3S$ beam are given in figures 4.5 to 4.6. At the separatrix the beam is attenuated to 40% of the initial beam intensity, see figure 4.5. De-excitation of the $2^3S$ into the ground state results in a strong rise of the ground-state population (2% of the initial beam intensity at the separatrix). Also, the $2^1S$ population shows a much stronger rise (maximum of $4{\cdot}10^{-3}$) compared to that of the initially pure ground-state beam (maximum of $4{\cdot}10^{-5}$, see figure 4.2). Figures 4.6 and 4.7 show singlet- and triplet-line intensities for a pure $2^3S$ beam. As expected, the triplet-line intensities of the $2^3S$ beam are much stronger than those resulting for the ground-state beam. In contrast to the $2^3S$-population density, the triplet-line intensities rise monotonously, whereas the singlet-line profiles reflect the progression of the $2^1S$ population density. The correlation between the line-intensity profiles and the electron-temperature profile is not as clearly visible as with the pure ground-state beam, especially in the case of the singlet lines.

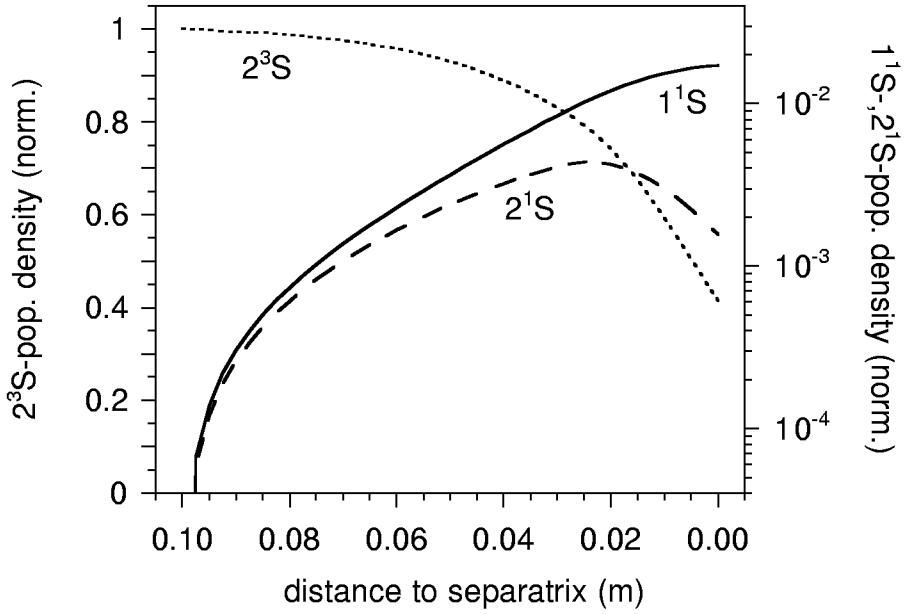


**Figure 4.5:** Progression of the $1^1S$-, $2^1S$-, and $2^3S$ populations for an initially pure $2^3S$ beam (normalized to the initial beam intensity). The modelling is based on AUG discharge #11277 and a 1 A / 30 keV He beam with 0.1 m diameter.

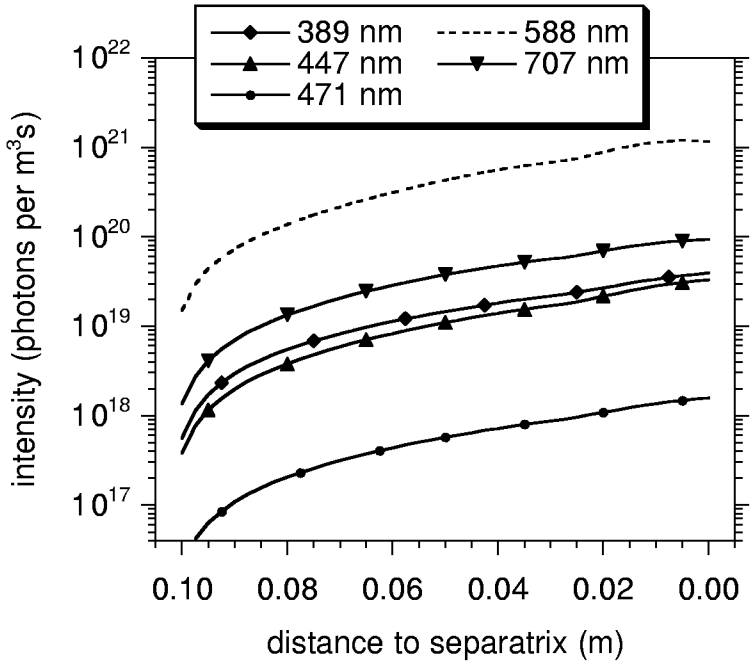


**Figure 4.6:** Progression of optical HeI-triplet lines for an initially pure $2^3S$ beam. The modelling is based on AUG discharge #11277 and a 1 A / 30 keV He beam with 0.1 m diameter.

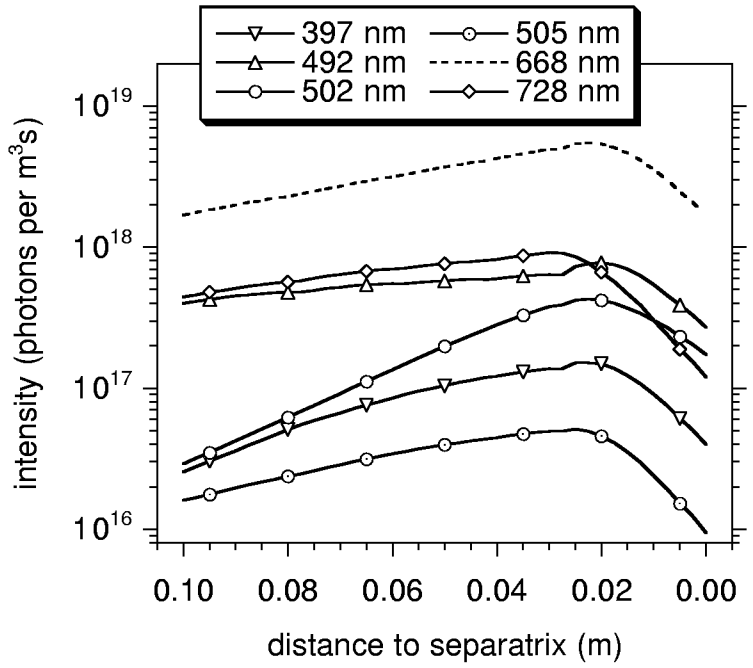


**Figure 4.7:** Progression of optical HeI-singlet lines for an initially pure $2^3S$ beam. The modelling is based on AUG discharge #11277 and a 1 A / 30 keV He beam with 0.1 m diameter.

#### 4.1.1.2 AUG Core Plasma

The $T_e$- and $n_e$ profiles used for the AUG core plasma calculations are shown in figure 4.8. As with the calculations for the plasma edge, a 30 keV He beam of 1 A equivalent current and 0.1 m diameter was considered.

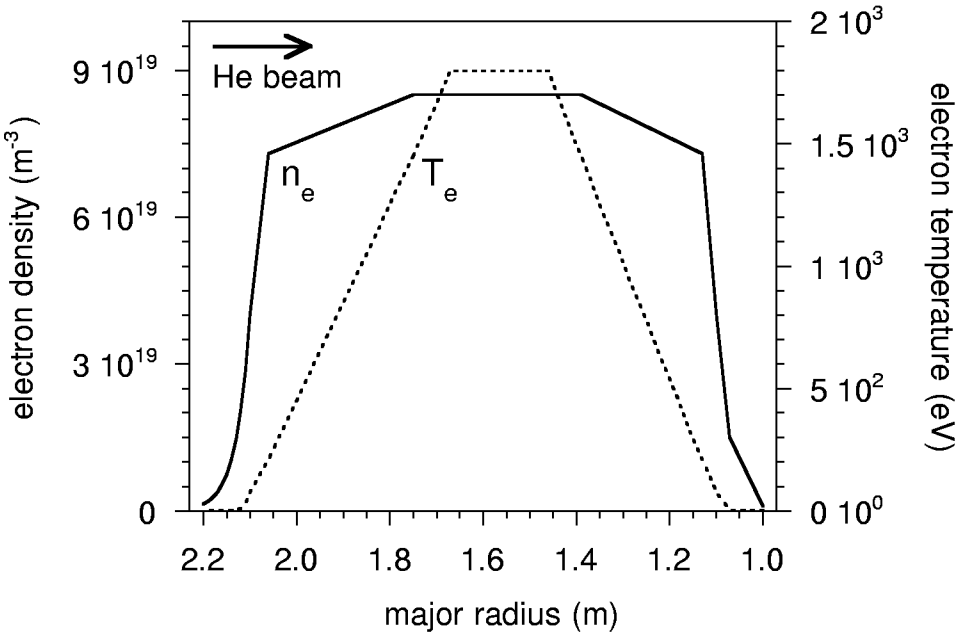


**Figure 4.8:** $n_e$- and $T_e$ profiles used for the modelling calculations for a typical AUG core plasma (discharge #11277).

Figure 4.9 shows the radial variation of the non-equilibrium level populations and selected singlet and triplet line-emission profiles for an initially pure $1^1$S- and an initially pure $2^3$S beam, respectively. Almost all line-intensity profiles of either spin system have the same shape inside the separatrices. Hence, only the most intense lines of each spin system are represented. The 728 nm line-intensity profile differs a little from the other singlet line-intensity profiles. For an illustration of these differences, the progression of the singlet-line intensities are shown in figures 4.10 and 4.11.

After passing the entire plasma the initially pure $1^1$S beam is attenuated to 6% of its incident current density. As observed in the plasma edge, the $2^1$S-population density is strongly coupled to the $1^1$S-population density. The $2^3$S-population density shows a quite different behaviour. The $2^3$S state is preferably populated in regions with low electron temperature (near the outer and inner separatrix at a major radius of 2.1 m and 1.1 m, respectively),

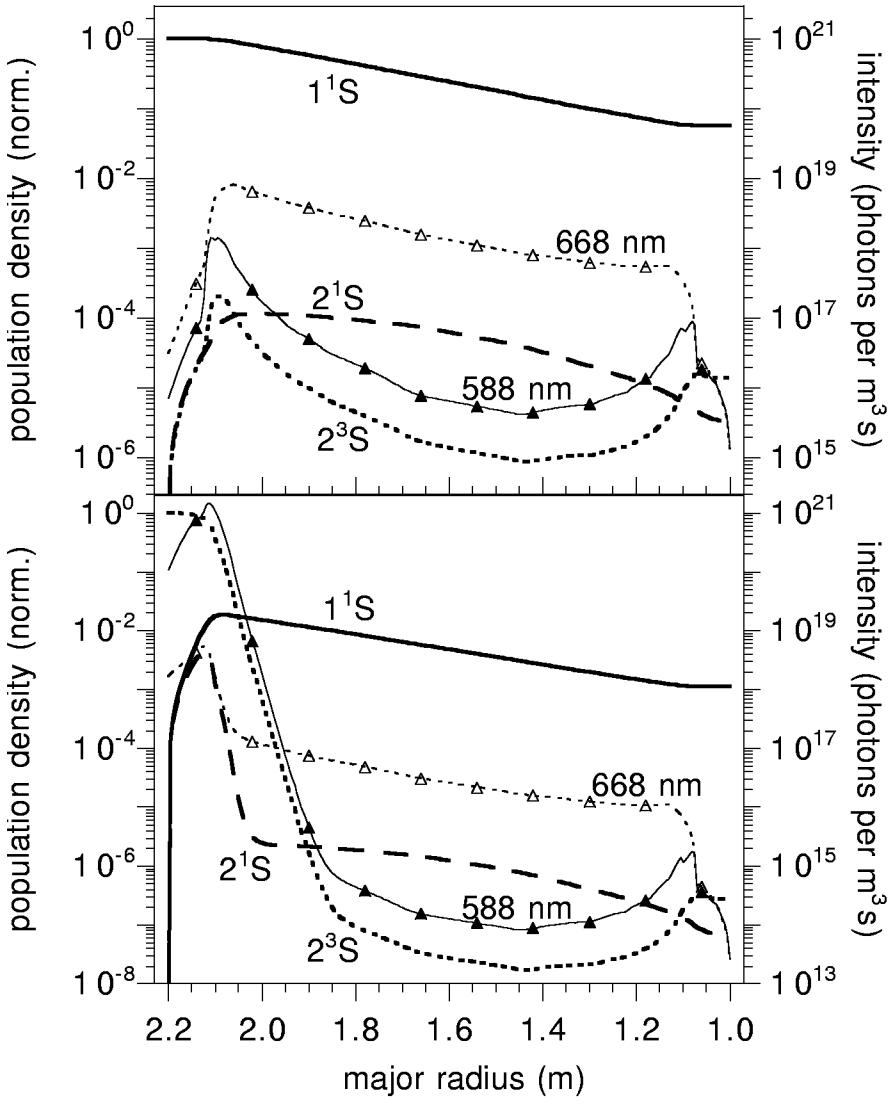


**Figure 4.9:** Progression of the $1^1$S-, $2^1$S- and $2^3$S populations (normalized to the initial beam intensity) and the most intense singlet (668 nm)- and triplet (588 nm) lines for an initially pure $1^1$S- (top) and $2^3$S beam (bottom), respectively. The modelling is based on AUG discharge #11277 and a 1 A / 30 keV He beam with 0.1 m diameter.

but strongly depopulated in the hot core. The triplet-line profiles are quite similar to the $2^3$S population-density profiles. In figure 4.10 all calculated singlet line-intensity profiles are shown. As observed in the plasma edge (cf. figures 4.4 and 4.2), progression of the $2^1$S-population density is represented best by the 728 nm-emission line, see figures 4.9 and 4.10.

The initially pure $2^3$S beam decays with an e-folding length of 17 mm (see figure 4.9). Only a few mm inside the separatrix, the ground-state population density reaches its maximum of

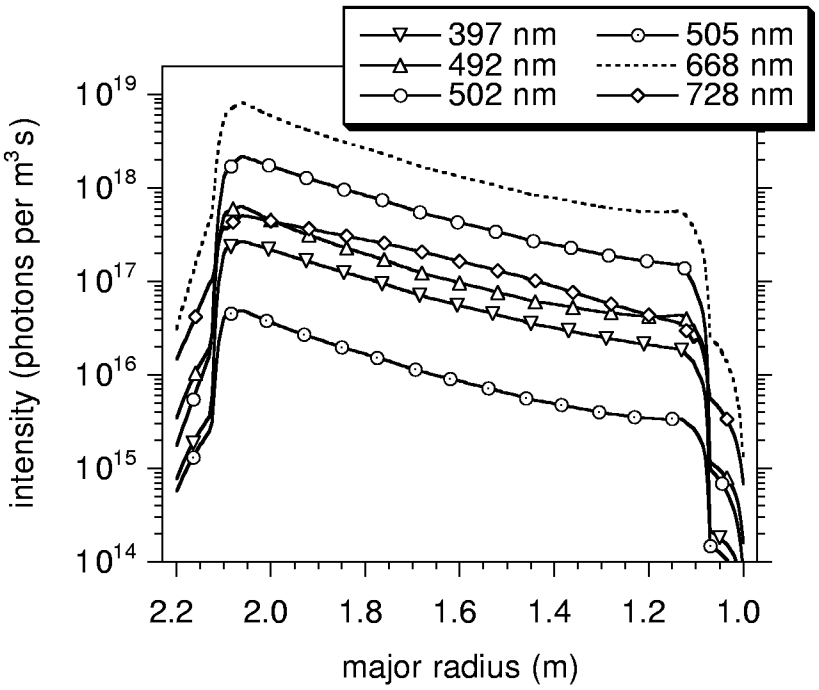


**Figure 4.10:** Progression of optical HeI-singlet lines for an initially pure $1^1S$ beam. The modelling is based on AUG discharge #11277 and a 1 A / 30 keV He beam with 0.1 m diameter.

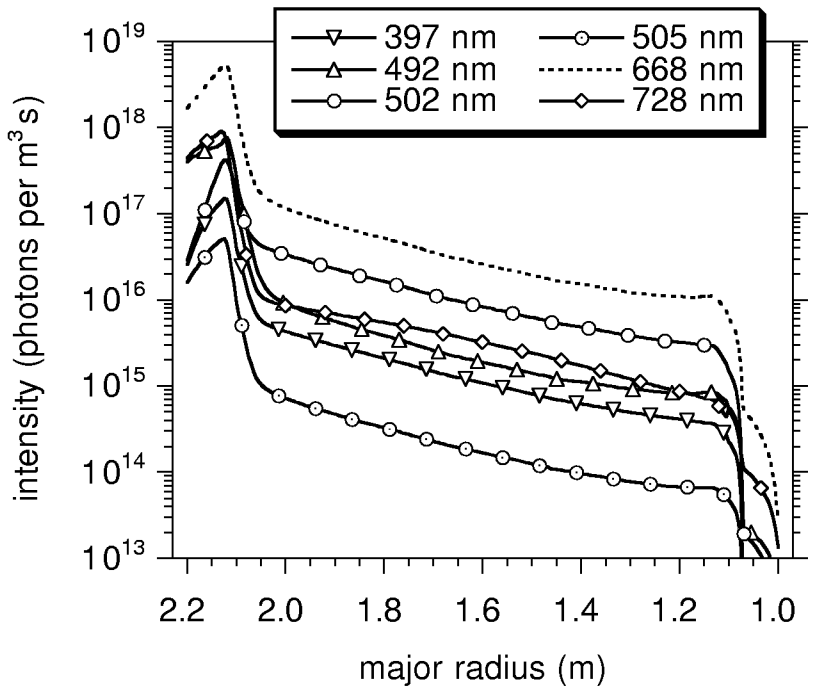


**Figure 4.11:** Progression of optical HeI-singlet lines for an initially pure $2^3S$ beam. The modelling is based on AUG discharge #11277 and a 1 A / 30 keV He beam with 0.1 m diameter.

0.02% of the initial beam intensity. As long as the $2^3$S concentration outnumbers the ground-state concentration, the progression of the $2^1$S-population density is dominated by the $2^3$S-population density. In the opposite case the $2^1$S-population density is strongly coupled to the ground state. After about 0.3 m a population-density composition independent from the initial beam composition is reached. This means that for such a situation the initial beam composition has no influence on the beam composition in most parts of the core plasma. For an initially pure $2^3$S beam the $2^3$S concentration in the plasma core is by almost two orders of magnitude lower than in the case of an initially pure ground state beam. This surprising result can be explained by the strong beam attenuation by ionization in the case of the pure $2^3$S beam, reducing the beam flux by two orders of magnitude within the first 0.1 m. Again, the line intensity profiles reflect the corresponding metastable state profiles. In figure 4.11 the singlet-line intensity profiles for the initially pure $2^3$S beam are shown. Once more, the 728 nm-emission line represents best the progression of the $2^1$S-population density.

### 4.1.2 JET Plasma

For a typical JET plasma we have chosen the H-mode discharge #42676 with a line-averaged density of $3.6{\cdot}10^{20}$ m$^{-2}$ and a peak electron temperature of 5 keV as inputs for our modelling. The calculations have been performed for an initial beam composition with pure ground state and pure metastable triplet state, respectively.

#### 4.1.2.1 JET Plasma Edge

The $T_e$- and $n_e$ profiles used for the JET plasma-edge calculations are shown in figure 4.12. The modelling parameters are as follows:

| | |
|---|---|
| beam energy | 80 keV |
| initial equivalent He beam current | 1 A |
| beam diameter | 0.1 m |
| $T_e$ at separatrix | 200 eV |
| $T_e$ decay length | 30 mm |
| $n_e$ at separatrix | $4{\cdot}10^{18}$ m$^{-3}$ |
| $n_e$ decay length | 30 mm |
| number of calculation steps | 200 |
| penetration depth | 0.1 m |

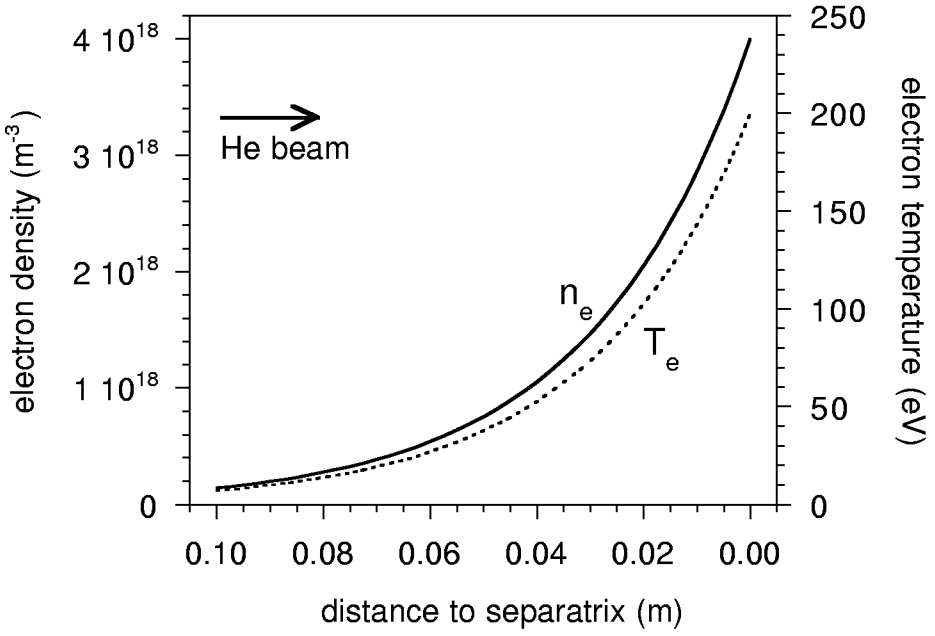


**Figure 4.12:** $n_e$- and $T_e$ profiles used for the modelling calculations for a typical JET edge plasma (discharge #42676).

The results for the population density- and the line intensity profiles for the initially pure ground-state beam are given in figures 4.13 to 4.15. At the separatrix only 0.35% of the initial beam intensity is already attenuated, see figure 4.13. The $2^1$S-population density shows a similar behaviour to in the AUG case (slower beam, lower $n_e$- and $T_e$ profiles), and the $2^1$S-population density at the separatrix is about one order of magnitude lower than in the AUG case. Due to the high $T_e$ most of the triplet-line profiles already starts to decrease a few cm outside the separatrix (see figure 4.14). Figure 4.15 shows the singlet lines for the initially pure ground-state beam. At the separatrix they have not yet reached their maximum intensity. Compared to the AUG predictive calculations, the line intensities of both the triplet- and singlet system for these calculations for an 80 keV beam penetrating a JET plasma are lower than for the AUG calculations for a 30 keV beam penetrating a less dense plasma.

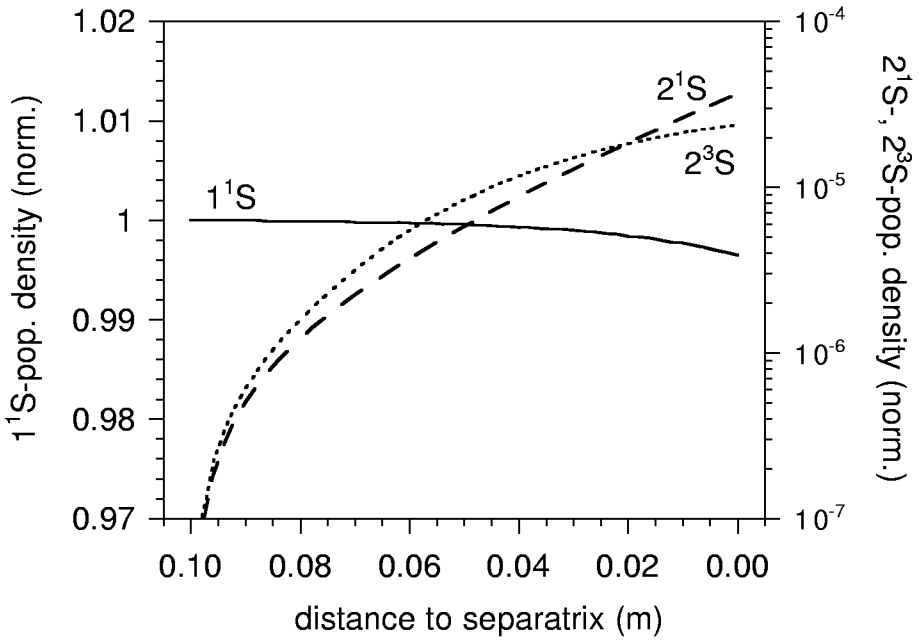


**Figure 4.13:** Progression of the $1^1$S-, $2^1$S-, and $2^3$S populations for an initially pure $1^1$S beam. The modelling is based on JET discharge #42676 and a 1 A / 80 keV He beam with 0.1 m diameter.

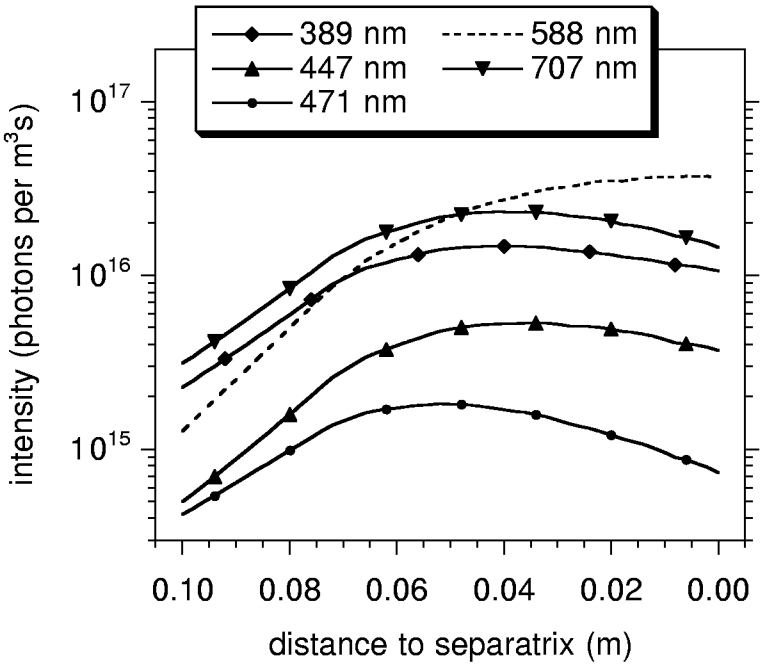


**Figure 4.14:** Progression of optical HeI-triplet lines for an initially pure $1^1$S beam. The modelling is based on JET discharge #42676 and a 1 A / 80 keV He beam with 0.1 m diameter.

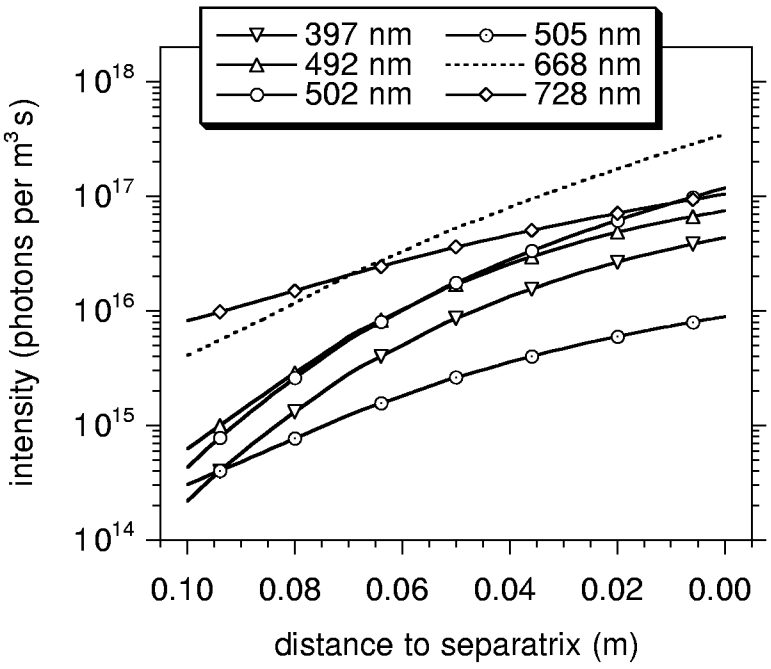


**Figure 4.15:** Progression of optical HeI-singlet lines for an initially pure $1^1$S beam. The modelling is based on JET discharge #42676 and a 1 A / 80 keV He beam with 0.1 m diameter.

The results for the population density- and the line intensity profiles for the initially pure $2^3$S beam are given in figures 4.16 to 4.18. At the separatrix only 5% of the initial beam intensity is attenuated, see figure 4.16. The rise of the ground state population ($2{\cdot}10^{-4}$ at the separatrix) due to de-excitation of the $2^3$S is much weaker than in the AUG case. The $2^1$S population shows a higher rise ($7{\cdot}10^{-5}$ at separatrix) compared to that of the initially pure ground-state beam ($4{\cdot}10^{-5}$ at separatrix, see figure 4.13). The $2^1$S-population density is much weaker than in the AUG case (cf. figure 4.5: $1{\cdot}10^{-3}$ at separatrix). Figures 4.17 and 4.18 show singlet- and triplet line intensities for a pure $2^3$S beam. As expected, the triplet line-intensity profiles are much more intense than the corresponding population densities in the case of a pure $1^1$S beam. In contrast to the $2^3$S population density, the triplet-line intensities rise monotonously as in the AUG case. Here, most of the singlet-line intensities do not reflect the progression of the $2^1$S population density, since some of them show an almost constant (492 nm, 502 nm, and 668 nm) or even descending profile (505 nm and 728 nm).

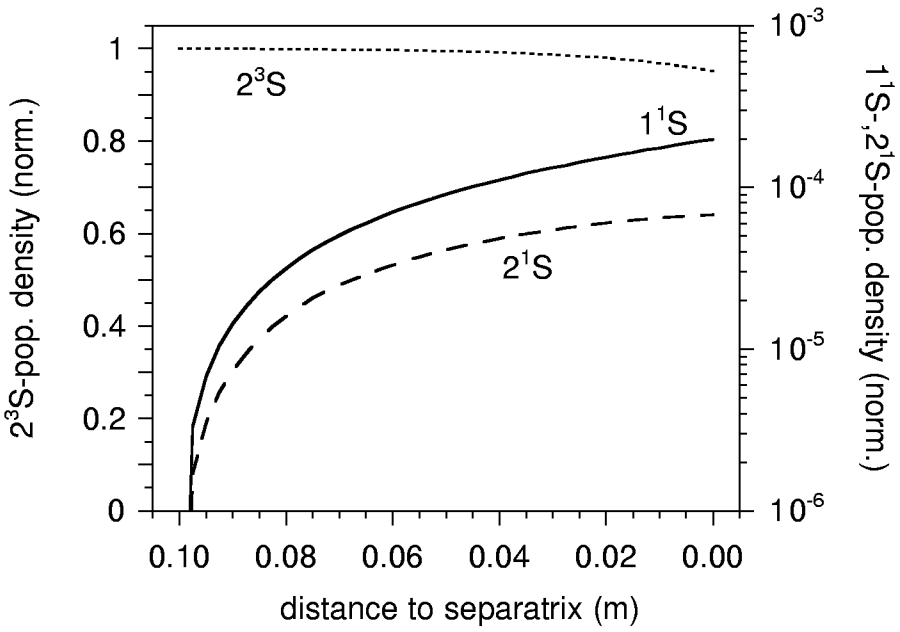


**Figure 4.16:** Progression of the $1^1$S-, $2^1$S-, and $2^3$S populations for an initially pure $2^3$S beam. The modelling is based on JET discharge #42676 and a 1 A / 80 keV He beam with 0.1 m diameter.

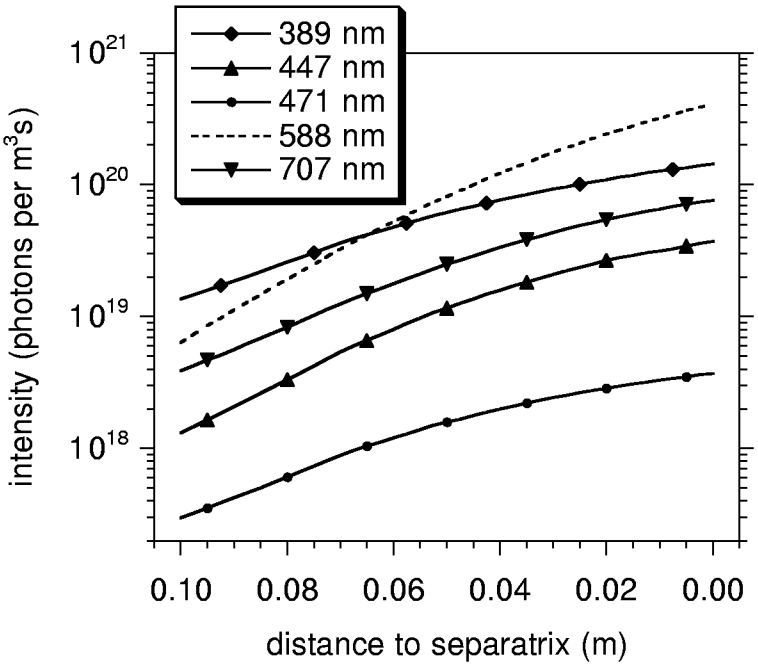


**Figure 4.17:** Progression of optical HeI-triplet lines for an initially pure $2^3$S beam. The modelling is based on JET discharge #42676 and a 1 A / 80 keV He beam with 0.1 m diameter.

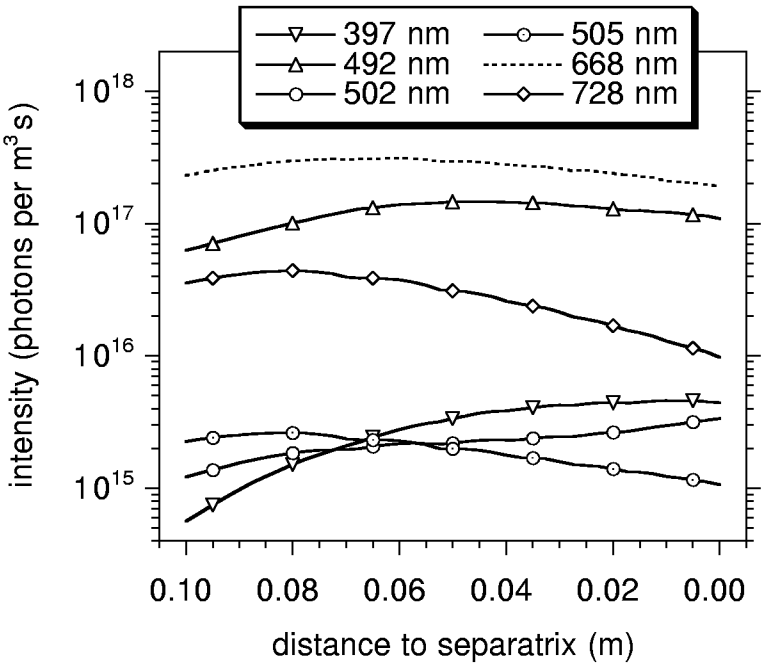


**Figure 4.18:** Progression of optical HeI-singlet lines for an initially pure $2^3$S beam. The modelling is based on JET discharge #42676 and a 1 A / 80 keV He beam with 0.1 m diameter.

#### 4.1.2.2 JET Core Plasma

The $T_e$- and $n_e$ profiles used for the JET core plasma calculations are shown in figure 4.19. As with the calculations for the plasma edge, an 80 keV He beam of 1 A equivalent current and 0.1 m diameter was considered.

Figure 4.20 shows the radial variation of the non-equilibrium level populations and selected singlet- and triplet line-emission profiles for an initially pure $1^1$S- and an initially pure $2^3$S beam, respectively. As almost all line-intensity profiles of each spin system show the same behaviour inside the core, only the most intense lines for both spin systems are represented. The singlet-line intensities for the initially pure $2^3$S beam show a different behaviour, which is displayed in figure 4.21.

After passing the entire plasma the initially pure $1^1$S beam is attenuated to only 40% of its incident current density. This compares with an attenuation to 5% for the predictive calculations for AUG with a slower beam, but lower $T_e$, $n_e$, and plasma diameter. As observed in the AUG case, the $2^1$S-population density is strongly coupled to the $1^1$S-population density, and the $2^3$S state is preferably populated in regions with low electron temperature (near the outer and inner separatrix at a major radius of 3.85 m and 2.1 m, respectively), but

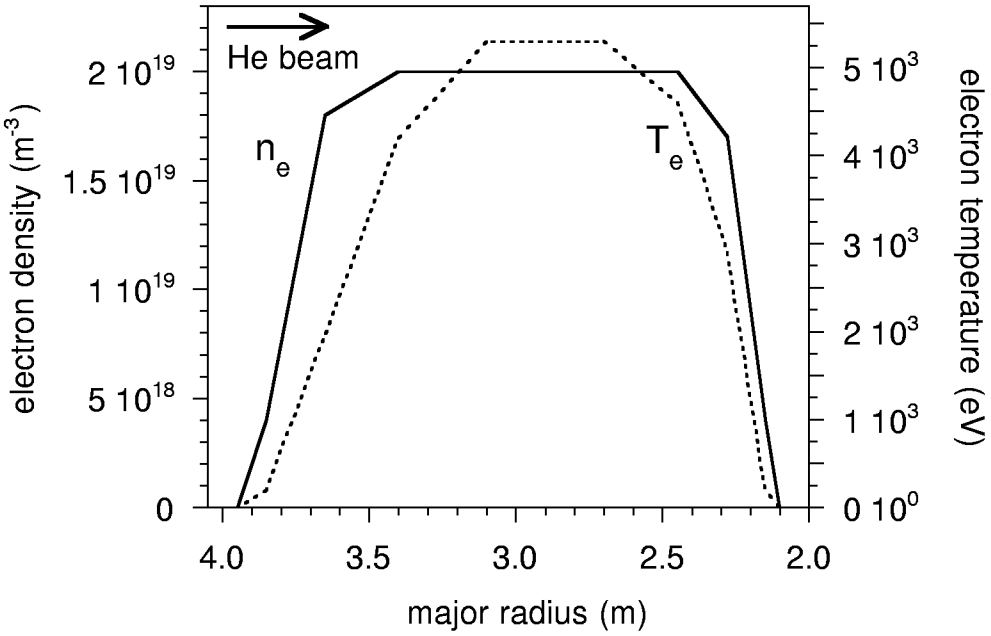


**Figure 4.19:** $n_e$- and $T_e$ profiles used for the modelling calculations for a typical JET core plasma (discharge #42676).

strongly depopulated in the hot core. As already mentioned, the line-intensity profiles are very similar to the corresponding metastable population-density profiles. The most intense lines of both spin systems are about one order of magnitude higher than those in the AUG case.

The initially pure $2^3$S beam decays with an e-folding length of 105 mm (see figure 4.20). This means that in this case the $2^3$S-population density does not reach saturation, in contrast to the AUG case. The progression of the triplet-line intensities inside the core is dominated by the decay of the $2^3$S-population density, and no effect of $T_e$ is observed at the inner separatrix. This leads us to the assumption that a high metastable fraction in the beam reduces the temperature sensitivity of the triplet lines (cf. chapter 4.2). About 0.2 m inside the separatrix, the ground-state population density reaches its maximum of 0.04% of the initial beam intensity, which is about 50 times smaller than for the AUG case.

As long as the $2^3$S concentration is by more than two orders of magnitude higher than the ground-state concentration, the progression of the $2^1$S-population density is dominated by the $2^3$S-population density. In the opposite case the $2^1$S-population density is strongly coupled to the ground state. Again, the 668 nm line-intensity profile shows the same behaviour as the $2^1$S-population density. In figure 4.21 all calculated singlet line-intensity profiles for the initially pure $2^3$S beam are given. In contrast to the pure $1^1$S beam and both the $1^1$S-

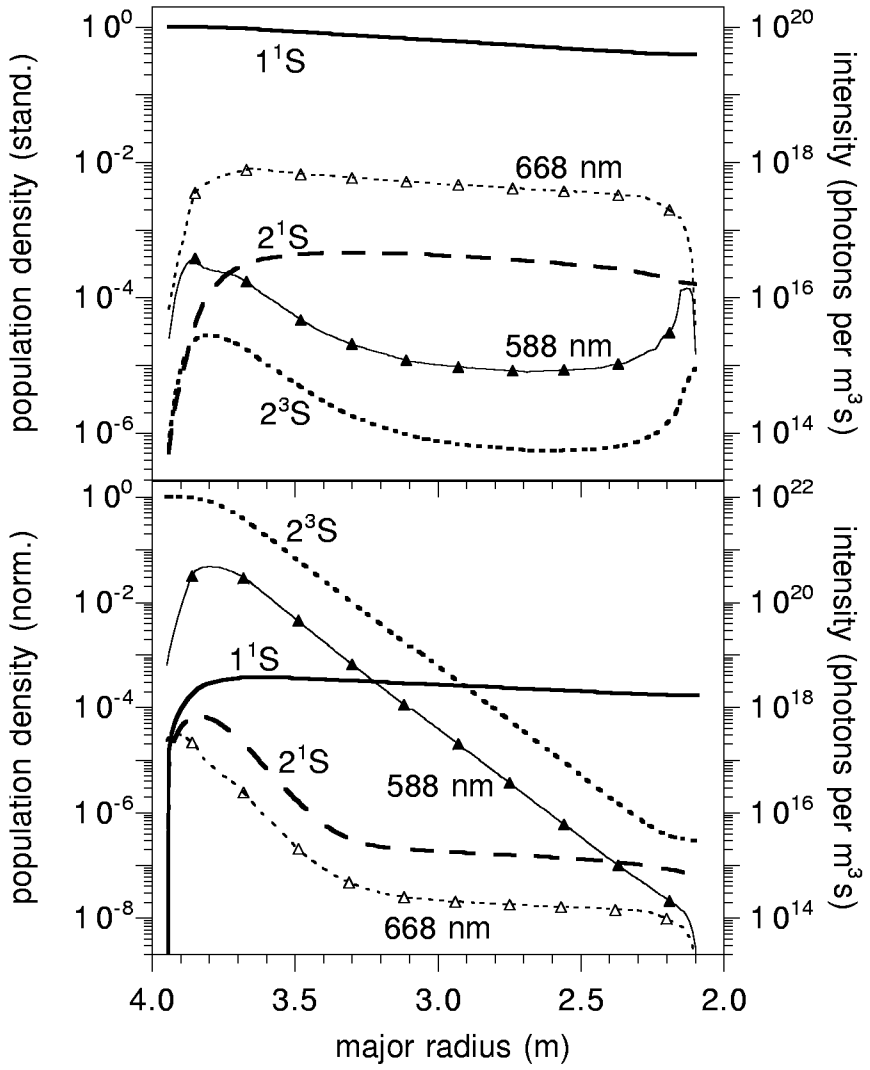


**Figure 4.20:** Progression of the $1^1$S-, $2^1$S- and $2^3$S populations (normalized to the initial beam intensity) and the most intense singlet (668 nm)- and triplet (588 nm) lines for an initially pure $1^1$S- (top) and $2^3$S beam (bottom), respectively. The modelling is based on JET discharge #42676 and a 1 A / 80 keV He beam with 0.1 m diameter.

and the $2^3$S beam calculated for AUG, the shapes of the singlet-line profiles differ from each other quite strongly. The 492 nm emission line ($4^1\mathrm{D} \rightarrow 2^1\mathrm{P}$) shows strongest coupling to the triplet system. In the region where the $2^1$S-population density has reached its saturation, the singlet-line intensities are about two orders of magnitude lower than for the AUG calculations.

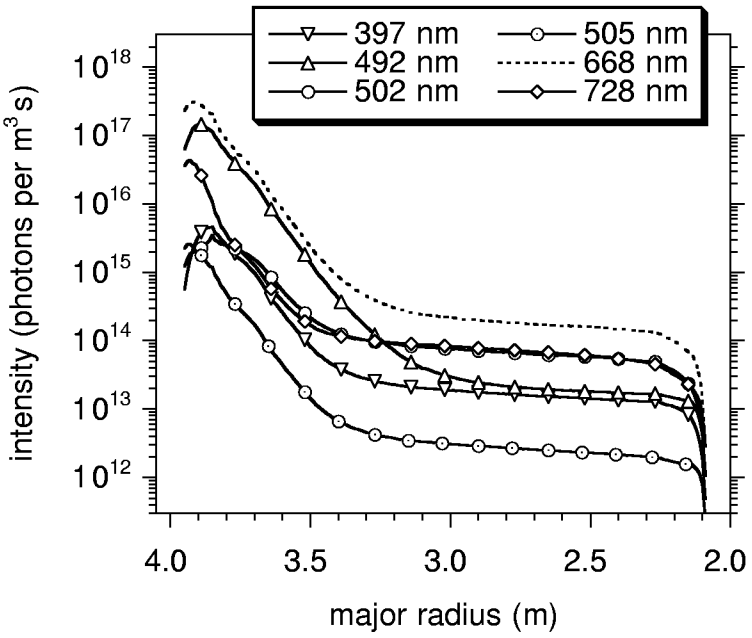


**Figure 4.21:** Progression of optical HeI-singlet lines for an initially pure $2^3$S beam. The modelling is based on JET discharge #42676 and a 1 A / 80 keV He beam with 0.1 m diameter.

### 4.1.3 Conclusions

The attenuation of a 80 keV He beam penetrating a hot, dense and rather large JET plasma is much weaker than that of a 30 keV He beam injected into a cooler and less dense ASDEX Upgrade plasma with its considerably smaller dimension. In both cases the progression of the singlet lines differs strongly from that of the triplet lines. The triplet states are preferably populated in regions with low electron temperature, i.e. near the outer and inner separatrices. Furthermore, the line-intensities for both spin systems show a quite different behaviour for the different scenarios. This leads to the assumption that the deduction of both $T_e$ and $n_e$ from singlet- and triplet line-intensity measurements is possible, especially with a pure ground-state beam. For a more systematic examination we have studied how the considered emission lines depend on $T_e$ and $n_e$, as will be presented in chapter 4.2.

Since in the case of a high initial $2^3$S fraction the triplet line-intensity profiles are dominated by the strong exponential drop of the $2^3$S-population density, we have to assume that the dependence of the triplet lines on the plasma parameter profiles is dramatically reduced. Also, the singlet lines are affected to some extent by the strong depopulation of the triplet system. Hence, our study presented in chapter 4.2 also deals with the consequence of an initial $2^3$S fraction on the sensitivity of line intensities to $T_e$ and $n_e$, respectively.

## 4.2 Sensitivity Study for $n_e$- and $T_e$ dependences

In order to assess the potential of He-beam emission for a useful plasma diagnostics, we have examined the sensitivity of the earlier discussed emission lines (chapter 3.4, table 3.1) with respect to $T_e$ and $n_e$. Based on profiles from a JET ITB discharge, we have calculated the line emission profiles for smooth $T_e$- and $n_e$ profiles and for profiles with either $n_e$- or $T_e$ steps in the plasma edge- and core region. As in chapter 4.1.2 a beam with energy of 80 keV, equivalent current of 1 A, and diameter of 0.1 m was chosen.

### 4.2.1 Plasma Edge and Pedestal

The $T_e$- and $n_e$ profiles used for the following sensitivity-study calculations for the plasma edge and pedestal are based on discharge #40554. The edge profiles are taken from the scrape-off layer database:

| | |
|---|---|
| $T_e$ at separatrix | 100 eV, |
| $T_e$ decay length | 17 mm, |
| $n_e$ at separatrix | $1.05{\cdot}10^{19}$ m$^{-3}$, |
| $n_e$ decay length | 12 mm, |
| location of separatrix | $R_{maj}^{outer} = 3.9$ m, $R_{maj}^{inner} = 2.1$ m. |

$T_e$- and $n_e$ profiles inside the separatrix are taken from LIDAR measurements and, if required, extrapolated to the value at the separatrix as given above. For the calculations we have used either these smooth profiles or profiles with constant sections and steps as shown in figure 4.22.

Calculations have been performed for 3 different scenarios:

- smooth $T_e$- and $n_e$ profiles,
- smooth $T_e$ profiles, $n_e$ steps,
- smooth $n_e$ profiles, $T_e$ steps.

Both ground-state He beams and He beams with 10% initial $2^3$S fraction have been modelled. The results for beams with 10% $2^3$S fraction are given in figures 4.23 to 4.28. Figures 4.23 and 4.24 show line-intensity profiles for smooth $n_e$- and $T_e$ profiles, figures 4.25 and 4.26 the

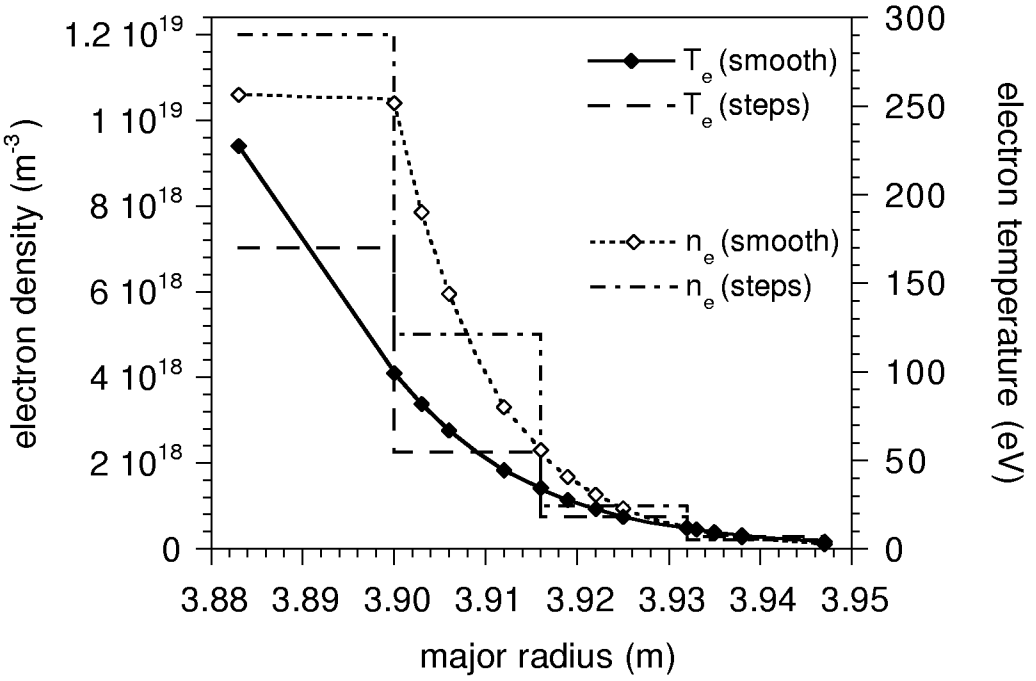


**Figure 4.22:** $n_e$- and $T_e$ profiles used for the sensitivity study. The data for the smooth profiles is taken from JET scrape-off layer database and LIDAR measurements for discharge #40554.

ones for $n_e$ steps, and figures 4.27 and 4.28 the ones for $T_e$ steps. Comparison between first experimental results at JET (see chapter 5.2) and the corresponding calculations showed that calculated line intensities have to exceed $10^{16}$ photons $\mathrm{m}^{-3}\mathrm{s}^{-1}$ in order to be detected by the spectroscopic system. This limit is marked in the figures.

The intensity of the singlet lines is strongly correlated to $n_e$ as can be seen in figure 4.25. In particular, the profiles of the 668 nm- and 492 nm line have the same shape as the $n_e$ profiles. Both lines are not very sensitive to $T_e$, as can also be seen in figure 4.27. The 668 nm line appears in the highest intensity which makes it a prime candidate for deriving $n_e$ profiles from emission profiles.

To deduce the $T_e$ profile from line-emission profiles, lines which are primarily sensitive to $T_e$ would be desireable. Unfortunately, all lines are too sensitive with respect to $n_e$ for being suitable for $T_e$ profile deduction on their own. Some singlet lines show a strong sensitivity to $T_e$, e.g. the 728 nm line which is the second strongest singlet line. The 389 nm triplet line shows the strongest sensitivity to $T_e$.

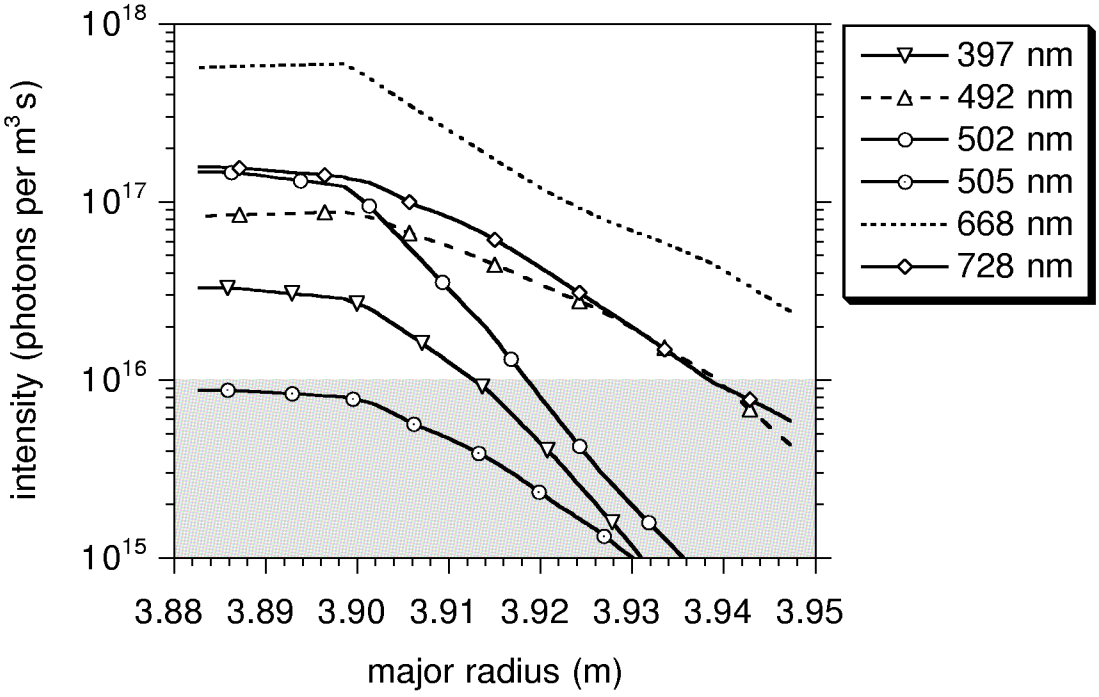


**Figure 4.23:** Singlet line-intensity profiles for smooth $n_e$- and $T_e$ profiles and an initial $2^3$S fraction of 10%.

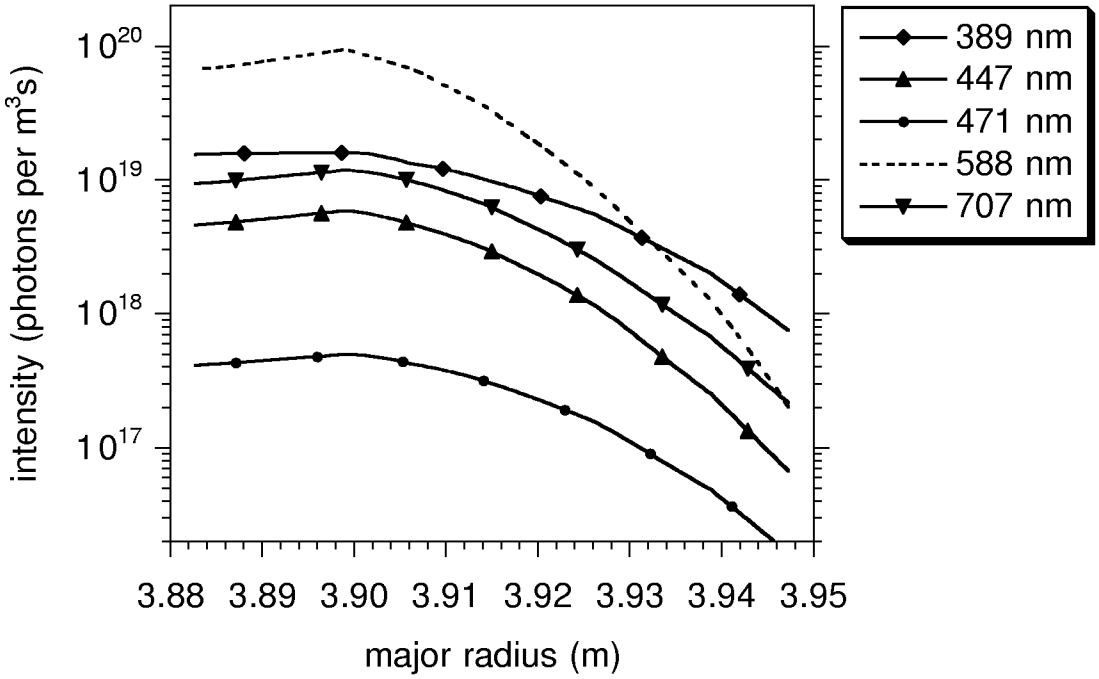


**Figure 4.24:** Triplet line-intensity profiles for smooth $n_e$- and $T_e$ profiles and an initial $2^3$S fraction of 10%.

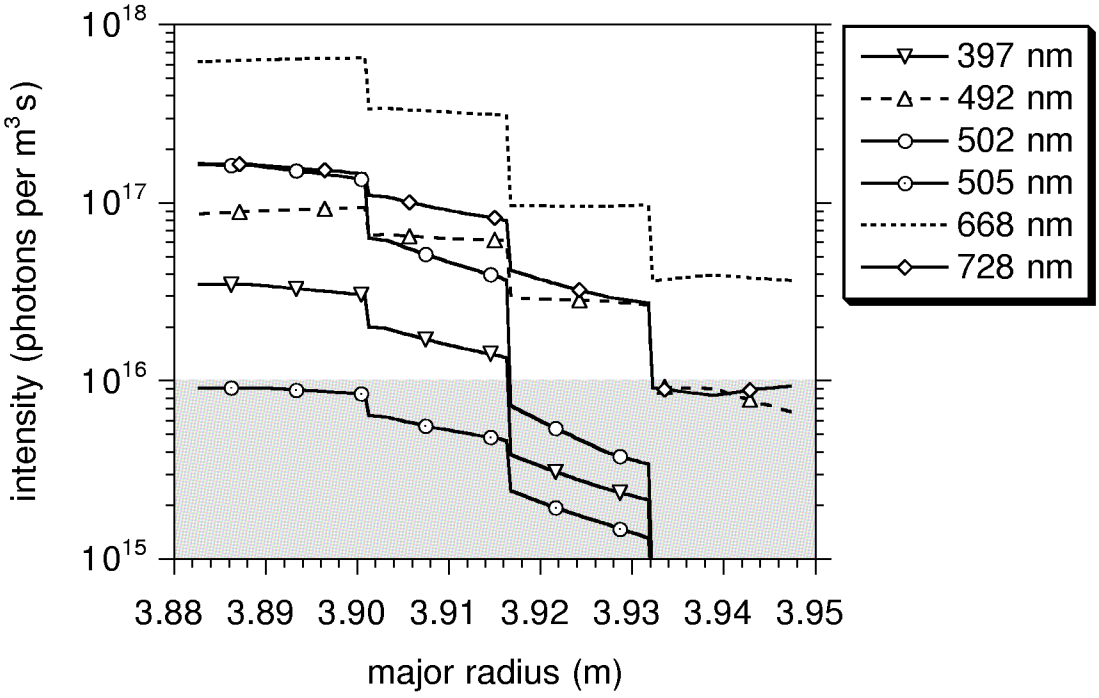


**Figure 4.25:** Singlet line-intensity profiles for profiles with $n_e$ steps and an initial $2^3$S fraction of 10%.

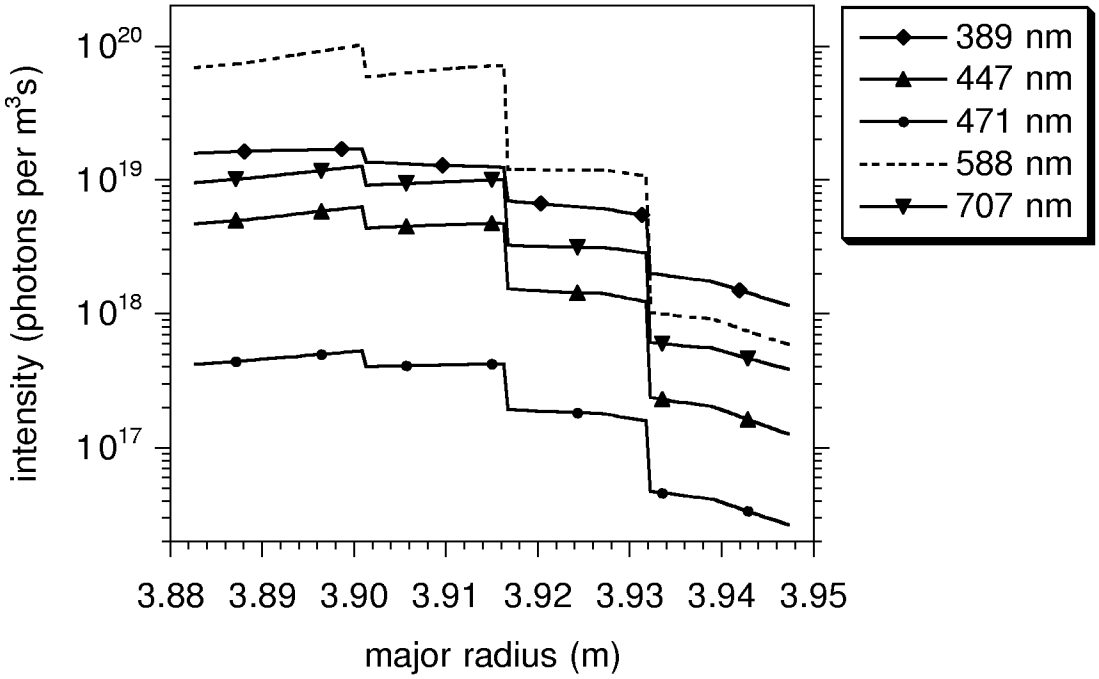


**Figure 4.26:** Triplet line-intensity profiles for profiles with $n_e$ steps and an initial $2^3$S fraction of 10%.

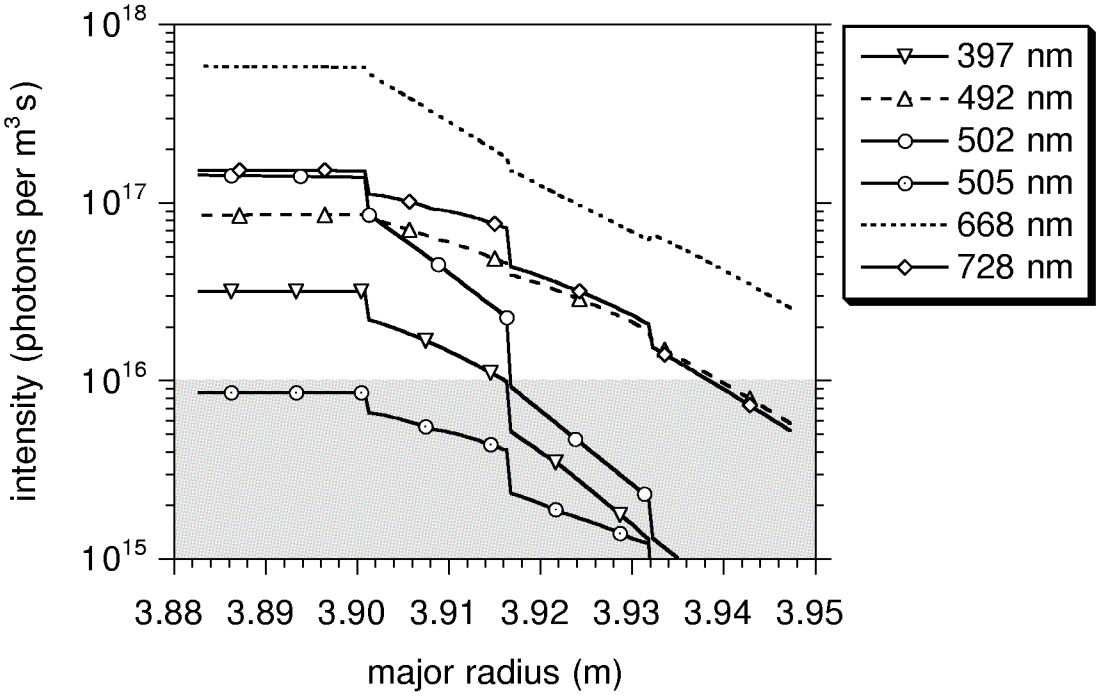


**Figure 4.27:** Singlet line-intensity profiles for profiles with $T_e$ steps and an initial $2^3$S fraction of 10%.

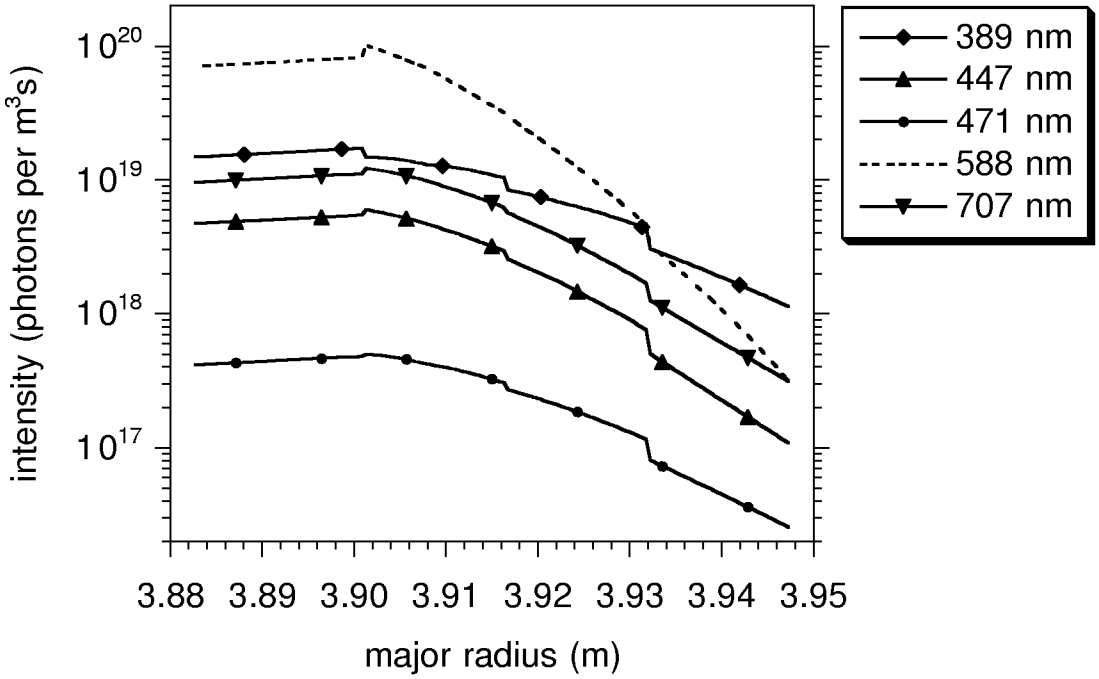


**Figure 4.28:** Triplet line-intensity profiles for profiles with $T_e$ steps and an initial $2^3$S fraction of 10%.

In order to quantify the response of line emission to $n_e$- or $T_e$ steps, we have calculated the ratios $S_n$ and $S_T$ defined as

$$S_{n,j} = \left( \frac{\Delta I/I}{\Delta n/n} \right)_j \tag{4.1}$$

and

$$S_{T,j} = \left( \frac{\Delta I/I}{\Delta T/T} \right)_j , \tag{4.2}$$

where $j$ defines particular $n_e$- or $T_e$ steps. $\Delta I/I$ is the relative intensity change, and the $\Delta n/n$ and $\Delta T/T$ give relative changes in $n_e$ and $T_e$, respectively.

The values of $S_n$ and $S_T$ for a pure ground-state He beam and a He beam with 10% initial $2^3$S fraction, respectively, are shown in tables 4.1 to 4.4. For better guidance, values exceeding $\pm 0.4$ are given in bold (high sensitivity to the considered parameter), whereas values between -0.15 and 0.15 are plotted in italic (low sensitivity to the considered parameter).

| major radius | $T_e$ in eV | $n_e$ in $10^{18}$ m$^{-3}$ | 397 nm | 492 nm | 502 nm | 505 nm | 668 nm | 728 nm |
|---|---|---|---|---|---|---|---|---|
| | | | $(\Delta I/I)/(\Delta n/n)$, 0% $2^3$S | | | | | |
| 3.932 m | 11.8 | 0.2 - 1.0 | **1.00** | **0.90** | **1.04** | **0.55** | **0.94** | **0.75** |
| 3.916 m | 34.3 | 1.0 - 5.0 | **0.80** | **0.72** | **1.00** | **0.43** | **0.91** | **0.45** |
| 3.901 m | 100 | 5.0 - 12 | **0.49** | **0.50** | **0.87** | 0.34 | **0.81** | 0.33 |
| | | | $(\Delta I/I)/(\Delta n/n)$, 10% $2^3$S | | | | | |
| 3.932 m | 11.8 | 0.2 - 1.0 | **1.13** | **0.72** | **1.00** | **0.63** | **0.69** | **0.75** |
| 3.916 m | 34.3 | 1.0 - 5.0 | **0.82** | **0.52** | **1.00** | **0.46** | **0.78** | **0.45** |
| 3.901 m | 100 | 5.0 - 12 | **0.49** | **0.43** | **0.87** | 0.34 | **0.77** | 0.33 |

**Table 4.1:** Relative emission-intensity changes for $n_e$ steps for all considered singlet lines of a pure ground-state He beam and a He beam with 10% initial $2^3$S fraction, respectively.

Basically all singlet lines are rather sensitive to changes in $n_e$, with $S_n$ values varying between 0.33 and 1.13, see table 4.1. At the separatrix $S_n$ can become relatively small, e.g. 0.33 for the 728 nm line and 0.34 for the 505 nm line. An initial $2^3$S fraction of 10% has little impact on the sensitivity to $n_e$. The 668 nm line is very sensitive to $n_e$ and has almost identical $S_n$ values for all three steps. As already noted (figure 4.25), the 668 nm line is the strongest singlet line and would be an ideal candidate for $n_e$ measurements.

| major radius | $T_e$ in eV | $n_e$ in $10^{18}$ m$^{-3}$ | 389 nm | 447 nm | 471 nm | 588 nm | 707 nm |
|---|---|---|---|---|---|---|---|
| | | | $(\Delta I/I)/(\Delta n/n)$, 0% $2^3$S | | | | |
| 3.932 m | 11.8 | 0.2 - 1.0 | **0.75** | **0.95** | **0.57** | **1.22** | **0.90** |
| 3.916 m | 34.3 | 1.0 - 5.0 | **0.51** | **0.69** | 0.30 | **1.08** | **0.64** |
| 3.901 m | 100 | 5.0 - 12 | 0.31 | 0.40 | 0.20 | **0.67** | 0.32 |
| | | | $(\Delta I/I)/(\Delta n/n)$, 10% $2^3$S | | | | |
| 3.932 m | 11.8 | 0.2 - 1.0 | **0.68** | **1.01** | **0.81** | **1.24** | **0.97** |
| 3.916 m | 34.3 | 1.0 - 5.0 | **0.41** | **0.76** | **0.55** | **1.07** | **0.76** |
| 3.901 m | 100 | 5.0 - 12 | 0.27 | **0.45** | 0.34 | **0.66** | **0.41** |

**Table 4.2:** Relative emission-intensity changes for $n_e$ steps for all considered triplet lines of a pure ground-state He beam and a He beam with 10% initial $2^3$S fraction, respectively .

The sensitivity of the triplet lines with respect to $n_e$ is given in table 4.2. Compared to the singlet lines, $S_n$ is much smaller for most of the triplet lines. The 588 nm line is the most sensitive one. In the outermost region the sensitivity of all triplet lines with respect to $n_e$ is relatively high. Towards the separatrix this sensitivity drops. An increase of the initial $2^3$S fraction has little impact on the sensitivity of the triplet lines. As for the singlet lines $S_n$ is relatively high for all triplet lines. The 389 nm line shows the smallest sensitivity and it is very intense.

| major radius | $T_e$ in eV | $n_e$ in $10^{18}$ m$^{-3}$ | 397 nm | 492 nm | 502 nm | 505 nm | 668 nm | 728 nm |
|---|---|---|---|---|---|---|---|---|
| | | | $(\Delta I/I)/(\Delta T/T)$, 0% $2^3$S | | | | | |
| 3.932 m | 7 - 18 | 1.0 | **1.67** | **6.01** | **8.61** | **4.92** | **2.54** | **2.61** |
| 3.916 m | 18 - 55 | 5.0 | **0.99** | **0.78** | **1.02** | **0.80** | **0.61** | **0.69** |
| 3.901 m | 55 - 170 | 12 | **0.45** | 0.22 | **0.48** | 0.33 | 0.14 | 0.34 |
| | | | $(\Delta I/I)/(\Delta T/T)$, 10% $2^3$S | | | | | |
| 3.932 m | 7 - 18 | 1.0 | **0.64** | 0.21 | **1.05** | **1.23** | *-0.14* | **0.49** |
| 3.916 m | 18 - 55 | 5.0 | **0.59** | *0.14* | **0.80** | **0.52** | *0.14* | **0.47** |
| 3.901 m | 55 - 170 | 12 | 0.34 | *0.05* | **0.44** | 0.25 | *0.05* | 0.29 |

**Table 4.3:** Relative emission-intensity changes for $T_e$ steps for all considered singlet lines of a pure ground-state He beam.

Results for $S_T$ for singlet lines are given in table 4.3. In the case of a pure ground-state beam the singlet lines show a larger sensitivity to $T_e$ than to $n_e$ for the two outermost steps, but this is dramatically reduced for the third step located at the separatrix. An increase in

the initial $2^3$S fraction results in a strong decrease in $S_T$. The lines at 492 nm- and 668 nm lose their sensitivity to $T_e$ almost entirely, $S_T$ of the 668 nm line even changes its sign, i.e. a sudden increase in temperature would result in a drop in emitted intensity (cf. figure 4.27). Additionally to its favourable sensitivity to $n_e$, the 668 nm line shows almost no sensitivity to $T_e$ confirming that this line is the prime candidate for $n_e$ measurements in the plasma edge.

| major radius | $T_e$ in eV | $n_e$ in $10^{18}$ m$^{-3}$ | 389 nm | 447 nm | 471 nm | 588 nm | 707 nm |
|---|---|---|---|---|---|---|---|
| | | | $(\Delta I/I)/(\Delta T/T)$, 0% $2^3$S | | | | |
| 3.932 m | 7 - 18 | 1.0 | **5.60** | **5.94** | **4.88** | **6.45** | **5.08** |
| 3.916 m | 18 - 55 | 5.0 | 0.15 | *0.07* | *0.07* | *0.03* | *0.05* |
| 3.901 m | 55 - 170 | 12 | **-0.53** | **-0.73** | **-0.67** | **-0.79** | **-0.69** |
| | | | $(\Delta I/I)/(\Delta T/T)$, 10% $2^3$S | | | | |
| 3.932 m | 7 - 18 | 1.0 | **0.59** | **0.77** | **0.61** | **0.66** | **0.50** |
| 3.916 m | 18 - 55 | 5.0 | 0.21 | *0.12* | *0.10* | *0.01* | *0.06* |
| 3.901 m | 55 - 170 | 12 | 0.16 | *-0.10* | *-0.04* | -0.24 | *-0.10* |
| | | | $(\Delta I/I)/(\Delta T/T)$, 1% $2^3$S | | | | |
| 3.932 m | 7 - 18 | 1.0 | **0.62** | **0.84** | **0.76** | **0.70** | **0.59** |
| 3.916 m | 18 - 55 | 5.0 | 0.20 | *0.12* | *0.10* | *0.01* | *0.06* |
| 3.901 m | 55 - 170 | 12 | 0.15 | *-0.12* | *-0.06* | -0.25 | *-0.12* |

**Table 4.4:** Relative emission-intensity changes for $T_e$ steps for all considered triplet lines of a pure ground-state He beam and a He beam with 10% and 1% initial $2^3$S fraction, respectively.

Table 4.4 shows the sensitivity of triplet lines to $T_e$. For a pure ground-state beam values of $S_T$ change dramatically from high positive at the outermost point to high negative at the separatrix. For all emission lines the absolute values for $S_T$ decrease with increasing initial $2^3$S fraction. For showing that this reduction in sensitivity already occurs for very small initial metastable fractions, an additional case with 1% $2^3$S fraction has been given in table 4.4. The same effect has also been pointed out by Brix [92]. Fast He beams used for the tokamak plasma experiments are produced by neutralization of fast He ions in gaseous targets ($H_2$, $D_2$, and He, see chapter 5). These neutral beams have at least a few % of metastable atoms. In spite of the lower sensitivity to $T_e$ for such a realistic metastable fraction the 389 nm line has a relatively constant sensitivity to $T_e$ which should be large enough for $T_e$ evaluation. Assuming that the $n_e$ profile is already known, it appears feasible to derive $T_e$ profiles from the 389 nm line using this $n_e$ profile and the emission profile as

inputs. Some of the singlet lines have comparable or even higher sensitivity to $T_e$ (397 nm, 502 nm, 505 nm, and 728 nm, cf. table 4.1). However, even the most intense one at 728 nm falls below the detection limit of the JET spectroscopic system in the outermost plasma region. Additionally, its sensitivity to $n_e$ is higher than for the 389 nm line. Hence, for $T_e$ measurements the emission line at 389 nm is recommended.

### 4.2.2 Core Region

The $n_e$- and $T_e$ profiles for our sensitivity test in the core region are based on JET discharge #40554 which developes an ITB. The profiles were taken from LIDAR measurements (ppf LIDR/NE, LIDR/TE) at 0.2 s (without ITB) and 0.7 s (with ITB) after the start of the high power phase. For our calculations we have used either profiles for which the LIDAR data is linearized within a few ranges, or profiles with constant sections and steps as shown in figures 4.29 and 4.30. Both $n_e$ and $T_e$ are quite high which causes a rather strong beam attenuation. The calculation showed that the beam will be attenuated in the plasma center to about 72% of its initial ground-state population density in case of the lower profiles (before ITB phase), whereas in case of the higher profiles (during ITB phase) the beam attenuation is about 64%.

Calculations have been performed for 6 different scenarios:

1. linearized $T_e$- and $n_e$ profiles before ITB phase,
2. same as 1. but with $n_e$ steps,
3. same as 1. but with $T_e$ steps,
4. linearized $T_e$- and $n_e$ profiles during ITB phase,
5. same as 4. but with $n_e$ steps,
6. same as 4. but with $T_e$ steps.

In order to quantify the response of the line emissions to $n_e$- or $T_e$ steps, we have calculated $S_n$ and $S_T$ (see equations 4.1 and 4.2) at each position with a $n_e$- or $T_e$ step.

The values of $S_n$ and $S_T$ (cf. equations 4.1 and 4.2) for a pure ground-state He beam and a He beam with an initial $2^3$S fraction of 10% are shown in tables 4.5 to 4.8. Once again, values exceeding $\pm 0.4$ are indicated in bold, those between -0.15 and 0.15 in italic, respectively.

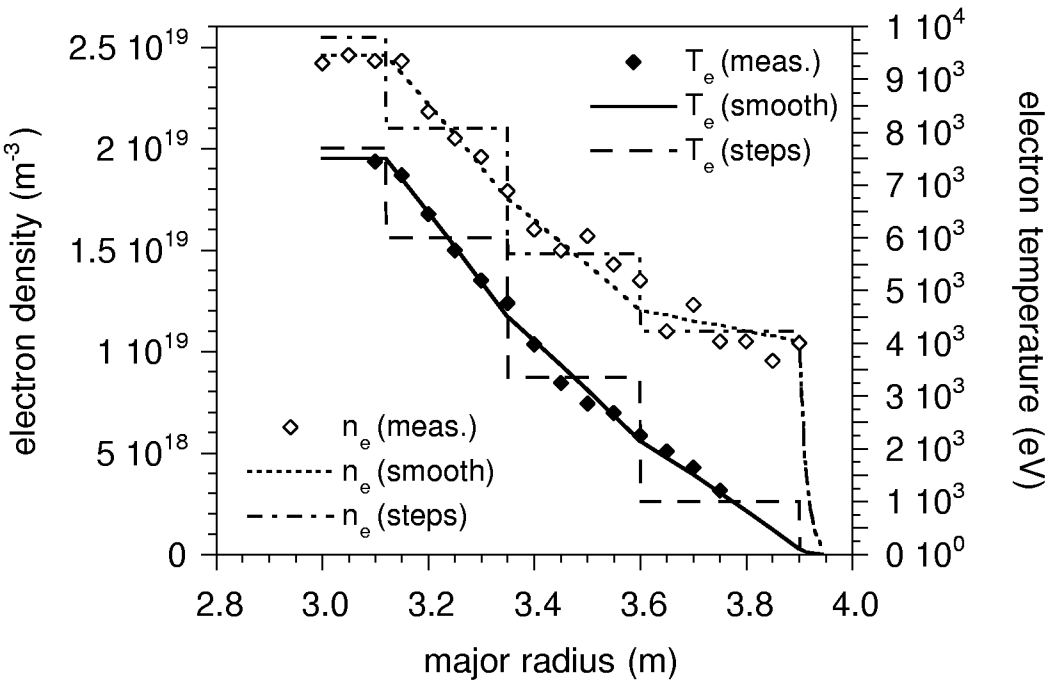


**Figure 4.29:** $n_e$- and $T_e$ profiles used for the sensitivity study of the JET core region. Data is taken from LIDAR measurements (JET discharge #40554) at 0.2 s after start of the high power phase.

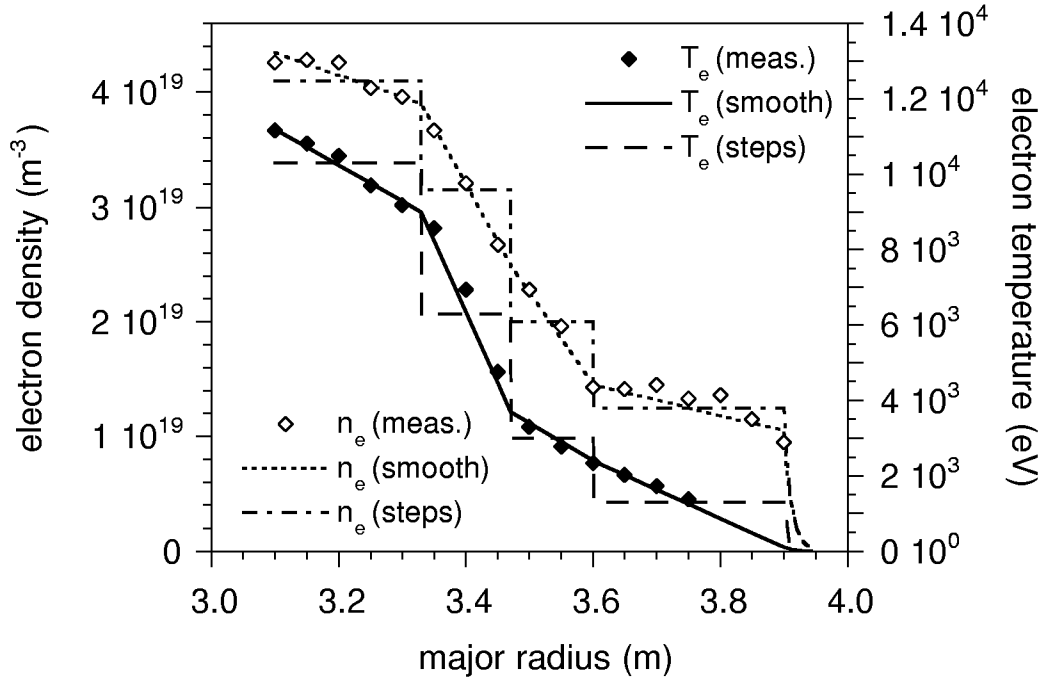


**Figure 4.30:** $n_e$- and $T_e$ profiles used for the sensitivity study of the JET core region. Data is taken from LIDAR measurements (JET discharge #40554) at 0.7 s after start of the high power phase.

| major radius | $T_e$ in keV | $n_e$ in $10^{19}$ m$^{-3}$ | 397 nm | 492 nm | 502 nm | 505 nm | 668 nm | 728 nm |
|---|---|---|---|---|---|---|---|---|
| | | | $(\Delta I/I)/(\Delta n/n)$ before ITB formation, 0% $2^3$S | | | | | |
| 3.60 m | 2.15 | 1.10 - 1.48 | **0.49** | **0.57** | **0.81** | **0.43** | **0.78** | **0.42** |
| 3.35 m | 4.50 | 1.48 - 2.10 | 0.39 | **0.50** | **0.78** | 0.29 | **0.76** | 0.27 |
| 3.12 m | 7.50 | 2.10 - 2.55 | 0.27 | **0.44** | **0.78** | *0.14* | **0.76** | *0.10* |
| | | | $(\Delta I/I)/(\Delta n/n)$ before ITB formation, 10% $2^3$S | | | | | |
| 3.60 m | 2.15 | 1.10 - 1.48 | **0.49** | **0.56** | **0.81** | **0.43** | **0.78** | **0.42** |
| 3.35 m | 4.50 | 1.48 - 2.10 | 0.39 | **0.50** | **0.78** | 0.29 | **0.76** | 0.27 |
| 3.12 m | 7.50 | 2.10 - 2.55 | 0.27 | **0.44** | **0.78** | *0.14* | **0.76** | *0.10* |
| | | | $(\Delta I/I)/(\Delta n/n)$ after ITB formation, 0% $2^3$S | | | | | |
| 3.60 m | 2.4 | 1.25 - 2.00 | **0.43** | **0.54** | **0.81** | 0.35 | **0.79** | 0.33 |
| 3.47 m | 3.7 | 2.00 - 3.15 | 0.26 | **0.42** | **0.77** | *0.12* | **0.75** | *0.09* |
| 3.33 m | 9.0 | 3.15 - 4.10 | 0.36 | **0.49** | **0.64** | 0.34 | **0.67** | 0.33 |
| | | | $(\Delta I/I)/(\Delta n/n)$ after ITB formation, 10% $2^3$S | | | | | |
| 3.60 m | 2.4 | 1.25 - 2.00 | **0.43** | **0.53** | **0.81** | 0.35 | **0.78** | 0.33 |
| 3.47 m | 3.7 | 2.00 - 3.15 | 0.26 | **0.42** | **0.77** | *0.12* | **0.75** | *0.09* |
| 3.33 m | 9.0 | 3.15 - 4.10 | 0.36 | **0.49** | **0.64** | 0.34 | **0.67** | 0.33 |

**Table 4.5:** Relative emission-intensity changes for $n_e$ steps for all considered singlet lines of a pure ground-state He beam and a He beam with 10% initial $2^3$S fraction, respectively.

Table 4.5 shows $S_n$ for all considered singlet lines. The $S_n$ for the singlet lines in the core region are smaller than in the edge region. Nevertheless, the sensitivity to $n_e$ is satisfactory. $S_n$ has values between 0.27 and 0.81 for all lines but at 505 nm and 728 nm. Occasionally $S_n$ can become rather weak, e.g. 0.09 for the 728 nm line and 0.12 for the 505 nm line. An initial $2^3$S fraction of 10% has almost no effect on $S_n$. The 502 nm-, 668 nm-, and 492 nm lines are the most sensitive ones with respect to $S_n$, showing only small variations over the whole core region. The 492 nm line is of much weaker intensity in the core than the other two lines (about by one order of magnitude lower than the 668 nm intensity). Hence, 502 nm and 668 nm are the prime candidates for deriving $n_e$ in the core region.

The sensitivity of the triplet lines with respect to $n_e$ is given in table 4.6. Compared to the singlet lines, $S_n$ is much smaller for most of the triplet lines with 588 nm line being the most sensitive one. In the outermost region the sensitivities of all triplet lines with respect to $n_e$ are relatively high. Towards the plasma center this sensitivity drops. In some cases $S_n$ even changes its sign, i.e. a sudden increase in temperature results in a drop in the emitted intensity (389 nm, 471 nm, and 707 nm). An increase of the initial $2^3$S fraction has little

| major radius | $T_e$ in keV | $n_e$ in $10^{19}$ m$^{-3}$ | 389 nm | 447 nm | 471 nm | 588 nm | 707 nm |
|---|---|---|---|---|---|---|---|
| | | | $(\Delta I/I)/(\Delta n/n)$ before ITB formation, 0% $2^3$S | | | | |
| 3.60 m | 2.15 | 1.10 - 1.48 | 0.32 | 0.39 | 0.33 | **0.52** | 0.36 |
| 3.35 m | 4.50 | 1.48 - 2.10 | *0.14* | 0.26 | 0.18 | **0.45** | 0.23 |
| 3.12 m | 7.50 | 2.10 - 2.55 | -0.17 | *0.02* | *-0.11* | 0.31 | *-0.01* |
| | | | $(\Delta I/I)/(\Delta n/n)$ before ITB formation, 10% $2^3$S | | | | |
| 3.60 m | 2.15 | 1.10 - 1.48 | 0.30 | 0.38 | 0.33 | **0.51** | 0.36 |
| 3.35 m | 4.50 | 1.48 - 2.10 | 0.15 | 0.25 | 0.17 | **0.46** | 0.23 |
| 3.12 m | 7.50 | 2.10 - 2.55 | *-0.13* | *0.04* | *-0.09* | 0.35 | *0.01* |
| | | | $(\Delta I/I)/(\Delta n/n)$ after ITB formation, 0% $2^3$S | | | | |
| 3.60 m | 2.4 | 1.25 - 2.00 | 0.23 | 0.33 | 0.25 | **0.52** | 0.30 |
| 3.47 m | 3.7 | 2.00 - 3.15 | *-0.13* | *0.05* | *-0.10* | 0.35 | *-0.02* |
| 3.33 m | 9.0 | 3.15 - 4.10 | 0.19 | 0.24 | 0.22 | 0.33 | 0.25 |
| | | | $(\Delta I/I)/(\Delta n/n)$ after ITB formation, 10% $2^3$S | | | | |
| 3.60 m | 2.4 | 1.25 - 2.00 | 0.22 | 0.33 | 0.26 | **0.51** | 0.31 |
| 3.47 m | 3.7 | 2.00 - 3.15 | *-0.14* | *0.06* | *-0.07* | 0.35 | *0.02* |
| 3.33 m | 9.0 | 3.15 - 4.10 | 0.17 | 0.22 | 0.19 | 0.30 | 0.21 |

**Table 4.6:** Relative emission-intensity changes for $n_e$ steps for all considered triplet lines of a pure ground-state He beam and a He beam with 10% initial $2^3$S fraction, respectively.

impact on the sensitivity of the triplet lines. To deduce $T_e$ profiles from line emission profiles, lines which are mainly sensitive to $T_e$ changes would be advantageous. Unfortunately, $S_n$ becomes relatively high for each triplet line at least for some $T_e/n_e$ combinations, as already observed in the edge region. The 389 nm- and 471 nm lines show the smallest sensitivity. The 471 nm line is the least intense one, whereas emission at 389 nm is very strong. Hence, the emission line at 389 nm would be most suitable for $T_e$ deduction provided its sensitivity to $T_e$ is not too small.

Results of $S_T$ for singlet lines are given in table 4.7. As with $S_n$, the sensitivities of the singlet lines with respect to $T_e$ are practically not effected at all by an increase for the initial $2^3$S fraction. Hence, only the results for the pure ground-state beam are presented in table 4.7. As expected, the singlet lines are not as sensitive to $T_e$ as to $n_e$. For most lines, $S_T$ is rather weak and decreases towards the plasma center. The 502 nm- and 492 nm lines have negative correlation to $T_e$ for all steps. The 502 nm line was suitable for deducing $n_e$ profiles because of its high sensitivity to $n_e$. In the edge region this line was not further considered due to its weak intensity. As this line has a rather small sensitivity to $T_e$ for all steps considered, it

| major radius | $T_e$ in keV | $n_e$ in $10^{19}$ m$^{-3}$ | 397 nm | 492 nm | 502 nm | 505 nm | 668 nm | 728 nm |
|---|---|---|---|---|---|---|---|---|
| | | | $(\Delta I/I)/(\Delta T/T)$ before ITB formation, 0% $2^3$S | | | | | |
| 3.60 m | 1.00 - 3.35 | 1.20 | *-0.09* | -0.26 | *-0.14* | *-0.11* | -0.25 | *0.14* |
| 3.35 m | 3.35 - 6.00 | 1.75 | *-0.07* | -0.21 | *-0.12* | *0.00* | *-0.17* | 0.23 |
| 3.12 m | 6.00 - 7.70 | 2.46 | *0.03* | *-0.06* | *-0.01* | *0.08* | *-0.02* | 0.21 |
| | | | $(\Delta I/I)/(\Delta T/T)$ after ITB formation, 0% $2^3$S | | | | | |
| 3.60 m | 1.3 - 3.0 | 1.45 | *-0.09* | -0.24 | *-0.14* | *-0.09* | -0.23 | *0.14* |
| 3.47 m | 3.0 - 6.3 | 2.50 | *-0.06* | -0.19 | *-0.11* | *0.00* | -0.15 | 0.22 |
| 3.33 m | 6.3 - 10.3 | 3.90 | *0.04* | *-0.06* | *0.00* | *0.10* | *-0.02* | 0.25 |

**Table 4.7:** Relative emission-intensity changes for $T_e$ steps for all considered singlet lines of a pure ground-state He beam.

looks most promising for deriving $n_e$ profiles in the core region. The 668 nm line which also has a high sensitivity to $n_e$, appears to be less suitable because of its higher $S_T$ value.

Table 4.8 shows the sensitivity of triplet lines with respect to $T_e$. In the case of a pure ground-state beam all values of $S_T$ are negative. As for the singlet lines, the absolute values of $S_T$ decrease towards the plasma center. Nevertheless, line emission at all wavelengths apart from line at 389 nm shows a useful sensitivity to $T_e$ for all steps. For all emission lines the absolute values for $S_T$ decrease with increasing initial $2^3$S fraction. As observed in the edge region, this reduction in sensitivity already occurs at very small initial metastable fractions as can be seen from the values for a beam with 1% $2^3$S fraction given in table 4.8. Nevertheless, both the 389 nm- (positive $S_T$) and the 588 nm emission line (negative $S_T$) for a beam with a few percent metastable fraction display rather constant sensitivities to $T_e$ which are large enough for useful evaluation. Since the 588 nm line is much more sensitive to $n_e$ than the 389 nm line, the latter one would be favourable for $T_e$ deduction in the core region.

### 4.2.3 Conclusions

The here presented sensitivity study showed that a He beam with an initial $2^3$S content is much less sensitive to $T_e$ than a pure ground-state beam. Since fast He beams produced by $He^+$ neutralization in a gaseous target always contain at least a few percent of metastable atoms, only results with a non-zero metastable fraction are relevant.

In order to derive from measured line-emission profiles the $T_e$- and $n_e$ profiles, such lines

| major radius | $T_e$ in keV | $n_e$ in $10^{19}$ m$^{-3}$ | 389 nm | 447 nm | 471 nm | 588 nm | 707 nm |
|---|---|---|---|---|---|---|---|
| | | | $(\Delta I/I)/(\Delta T/T)$ before ITB formation, 0% $2^3$S | | | | |
| 3.60 m | 1.00 - 3.35 | 1.20 | -0.15 | **-0.48** | **-0.64** | **-0.67** | **-0.70** |
| 3.35 m | 3.35 - 6.00 | 1.75 | *-0.01* | -0.33 | **-0.47** | **-0.59** | **-0.75** |
| 3.12 m | 6.00 - 7.70 | 2.46 | *0.00* | -0.19 | -0.25 | -0.36 | **-0.47** |
| | | | $(\Delta I/I)/(\Delta T/T)$ before ITB formation, 10% $2^3$S | | | | |
| 3.60 m | 1.00 - 3.35 | 1.20 | 0.17 | *0.01* | *0.00* | -0.24 | *-0.14* |
| 3.35 m | 3.35 - 6.00 | 1.75 | 0.20 | *0.11* | *0.08* | -0.20 | *-0.11* |
| 3.12 m | 6.00 - 7.70 | 2.46 | *0.12* | *0.10* | *0.07* | -0.16 | *-0.11* |
| | | | $(\Delta I/I)/(\Delta T/T)$ after ITB formation, 0% $2^3$S | | | | |
| 3.60 m | 1.3 - 3.0 | 1.45 | *-0.14* | **-0.45** | **-0.60** | **-0.63** | **-0.67** |
| 3.47 m | 3.0 - 6.3 | 2.50 | *-0.03* | -0.33 | **-0.45** | **-0.57** | **-0.70** |
| 3.33 m | 6.3 - 10.3 | 3.90 | *-0.01* | -0.26 | -0.34 | **-0.48** | **-0.65** |
| | | | $(\Delta I/I)/(\Delta T/T)$ after ITB formation, 10% $2^3$S | | | | |
| 3.60 m | 1.3 - 3.0 | 1.45 | 0.16 | *0.03* | *0.01* | -0.21 | *-0.12* |
| 3.47 m | 3.0 - 6.3 | 2.50 | 0.20 | *0.11* | *0.09* | -0.18 | *-0.09* |
| 3.33 m | 6.3 - 10.3 | 3.90 | 0.20 | 0.18 | *0.14* | *-0.12* | *-0.06* |
| | | | $(\Delta I/I)/(\Delta T/T)$ after ITB formation, 1% $2^3$S | | | | |
| 3.60 m | 1.3 - 3.0 | 1.45 | 0.16 | *0.02* | *0.01* | -0.21 | *-0.13* |
| 3.47 m | 3.0 - 6.3 | 2.50 | 0.20 | *0.11* | *0.08* | -0.19 | *-0.11* |
| 3.33 m | 6.3 - 10.3 | 3.90 | 0.20 | 0.17 | *0.13* | *-0.13* | *-0.08* |

**Table 4.8:** Relative emission-intensity changes for $T_e$ steps for all considered triplet lines of He beam with 0%, 1% and 10% initial $2^3$S fraction, respectively.

would be most suitable which are exclusively or at least predominantly sensitive to either $T_e$ or $n_e$, as in the case of thermal He beams [36]. For fast He beams (80 keV) there exists one line which is mainly sensitive to $n_e$, but no line which is predominantly sensitive to $T_e$.

It is thus expected that the density profile can be derived from the 668 nm line. If the sensitivity of the optical system can be enhanced, also the 492 nm line would be suitable. Once an $n_e$ profile is known it should be possible to calculate the related $T_e$ profile from any line with a sufficiently strong sensitivity to $T_e$, even if that line is also sensitive to $n_e$. The 389 nm line is the most sensitive one with respect to $T_e$. Although its sensitivity is still relatively small, it might be adequate for $T_e$ deduction. He beam emission spectroscopy, being a local diagnostics, could thus have potential in resolving strong local temperature gradients, even if its overall sensitivity to $T_e$ is much weaker than that to $n_e$. However, appropriate methods to derive $T_e$- and $n_e$ profiles from measured HeI emission profiles still have to be developed.